Annu. Rev. Astron. Astrophys. 2005. 43:677–725
doi: 10.1146/annurev.astro.43.051804.102221

First published online as a Review in Advance on July 1, 2005

MOLECULAR GAS AT HIGH REDSHIFT

P.M. Solomon
Department of Physics and Astronomy, State University of New York, Stony Brook, New York 11794; email: psolomon@sbastk.ess.sunysb.edu

P.A. Vanden Bout
National Radio Astronomy Observatory, Charlottesville, Virginia 22903; email: pvandenb@nrao.edu

Key Words early Universe, galaxies, starbursts, interstellar matter

■ **Abstract** The Early Universe Molecular Emission Line Galaxies (EMGs) are a population of galaxies with only 36 examples that hold great promise for the study of galaxy formation and evolution at high redshift. The classification, luminosity of molecular line emission, molecular mass, far-infrared (FIR) luminosity, star formation efficiency, morphology, and dynamical mass of the currently known sample are presented and discussed. The star formation rates derived from the FIR luminosity range from about 300 to 5000 $M_\odot$ year^{-1} and the molecular mass from 4×10^9 to 1×10^{11} $M_\odot$. At the lower end, these star formation rates, gas masses, and diameters are similar to those of local ultraluminous infrared galaxies and represent starbursts in centrally concentrated disks, sometimes, but not always, associated with active galactic nuclei. The evidence for large (>5 kpc) molecular disks is limited. Morphology and several high angular resolution images suggest that some EMGs are mergers with a massive molecular interstellar medium in both components. A critical question is whether the EMGs, in particular those at the higher end of the gas mass and luminosity distribution, represent the formation of massive, giant elliptical galaxies in the early Universe. The sample size is expected to grow explosively in the era of the Atacama Large Millimeter Array (ALMA).

1. INTRODUCTION

One of the many important advances in our knowledge of the distant, early Universe during the past decade has come from observations of spectral line emission from interstellar molecular gas, the raw material from which stars form, in high-redshift $z > 2$ galaxies. For convenience, we call these objects Early (Universe) Molecular (Line Emission) Galaxies (EMGs). The molecular interstellar medium (ISM) plays a critical role in the evolution of galaxies; these observations provide the first evidence of the location and mass of molecular clouds during the epoch of galaxy formation. To date, observations of rotational transitions of carbon monoxide (CO) have been reported for 36 sources with redshift $z > 1$, unequivocally demonstrating

that molecular clouds, an extreme Population I component, appeared early in the history of the Universe. (For completeness, we have included three galaxies with CO detection of $1 < z < 2$ in our review.) The jump from detecting CO in local ($z \leq 0.3$) galaxies to high-redshift observations was made possible by the increased sensitivity of millimeter-wave telescopes and arrays. It was also facilitated by the large masses of molecular gas associated with EMGs, a "negative K-correction" (see Section 7.1) for CO emission, gravitational lensing of many of the sources, and selection of sources with strong far-infrared (FIR) emission, which is often associated with star-forming molecular gas.

Almost all candidate galaxies successfully detected in high-redshift CO emission were first identified as strong FIR/submillimeter sources with FIR luminosity in excess of 10^{12} $L_{\odot}$. Given the relatively narrow instantaneous bandwidth of millimeter-wave receivers and spectrometers, an important selection criterion for CO line searches has been the availability of accurate redshifts from optical emission line spectroscopy. This situation changes as instrumental bandwidths increase.

Two main techniques have been applied to find most EMGs. The first employs large optical surveys of bright high-z quasars as a potential source list followed by observations of the flux at 1.2 mm or 0.85 mm. At these wavelengths the continuum of an EMG is dominated by thermal dust emission rather than an extension of the nonthermal radio continuum. CO emission has now been observed from 16 quasars, including the most distant known quasar at $z = 6.4$ (Walter et al. 2003). The second technique identifies highly luminous infrared (IR) galaxies from blank field observations with submillimeter-wave bolometers. Although not targeting individual cases of strong lensing, these observations often take advantage of intermediate-redshift cluster lensing. These techniques have led to the discovery of extremely luminous dusty FIR galaxies at high redshift, similar to local ultraluminous infrared galaxies (ULIRGs), but with a much higher space density. The search for CO in these submillimeter galaxies (SMGs) illustrates the (historical) importance of having good redshifts. Initial searches using Lyα redshifts were disappointing; later, the availability of Hα redshifts led to a success rate of >50%. A total of 11 SMGs have been reported as having CO emission. There are 73 SMGs with spectroscopic redshifts (Chapman et al. 2005), so a large number of CO detections are possible in the surveys under way. A third detection strategy involved searching IR-luminous radio galaxies for CO emission. Seven such detections have been reported. Finally, one Lyman Break galaxy (LBG) has been observed in CO emission, a detection made possible by strong magnification by a gravitational lens, and one extremely red object (ERO) has been detected.

The discovery of high-redshift CO emission predates these surveys. IRAS F10214 was a source at the detection limit of IRAS in the 60- and 100-μm bands, shown to be of high FIR luminosity when its redshift of $z = 2.3$ was (serendipitously) measured (Rowan-Robinson et al. 1991). The high FIR luminosity motivated a successful search for the rotational J = 3–2 line of CO with the NRAO 12-m Telescope (Brown & Vanden Bout 1991, 1992). The (3–2) detection was soon confirmed at the Institut de Radioastronomie Millimétrique (IRAM) 30-m

Telescope, but with a much smaller flux (Solomon, Downes & Radford 1992a), and the CO(6–5) line was also observed, indicating the presence of warm molecular gas typically associated with star formation. Successful searches for redshifted CO emission in several quasars soon followed: the Cloverleaf at $z = 2.6$ (Barvainis et al. 1994), BR1202 (Omont et al. 1996b) at $z = 4.7$, and BRI1335 at $z = 4.4$ (Guilloteau et al. 1997).

The CO observations of EMGs have the potential to answer several important questions about star formation and galaxy evolution in the early Universe: What is the mass of molecular gas and how does it compare with the dynamical mass? Are the EMGs centrally concentrated, as are most local ULIRGs, or are they extended protogalaxies with substantially more molecular mass than that of ULIRGs? What is the star formation lifetime? What is the final evolutionary state of the EMGs?

2. DEFINING THE EMGs

2.1. Luminosities: Basic Relations

The calculation of high-redshift source properties from the observation of molecular emission lines requires care with respect to the cosmology assumed. This is important when comparing published source properties, as different cosmologies can lead to significantly different values for properties such as luminosity, size, and mass. In this review we have assumed a cosmology with $\Omega_m = 0.3$, $\Omega_\Lambda = 0.7$, and $H_0 = 70$ km s^{-1} Mpc^{-1}.

The CO line luminosity can be expressed in several ways. From energy conservation, the monochromatic luminosity, observed flux density, and luminosity distance are related by $\nu_{rest} L(\nu_{rest}) = 4\pi D_L^2 \, \nu_{obs} S(\nu_{obs})$, yielding

$$L_{CO} = 1.04 \times 10^{-3} \, S_{CO} \, \Delta v \, \nu_{rest} (1+z)^{-1} \, D_L^2, \qquad (1)$$

where the CO line luminosity, L_{CO}, is measured in $L_\odot$; the velocity-integrated flux, $S_{CO} \, \Delta v$, in Jy km s^{-1}; the rest frequency, $\nu_{rest} = \nu_{obs}(1+z)$, in GHz; and the luminosity distance, D_L, in Mpc.[1]

The CO line luminosity is often expressed (Solomon et al. 1997) in units of K km s^{-1} pc^2 as the product of the velocity-integrated source brightness temperature, $T_b \, \Delta v$, and the source area, $\Omega_s D_A^2$, where Ω_s is the solid angle subtended by the source. The observed integrated line intensity, $I_{CO} = \int T_{mb} \, dv$, measures the beam diluted brightness temperature, which decreases with redshift,

[1]The rough dependence of the luminosity distance on redshift can be seen from the following: $D_L = D_A(1+z)^2$, where D_A is the angular size distance. For the cosmology assumed in this review, D_A rapidly increases with redshift, reaching a peak value at $z \approx 1.6$, and then declines roughly as $(1+z)^{-1}$ for larger z. So for redshifts larger than $z \sim 2$, D_L grows roughly as $(1+z)$. A calculator for computing luminosity and angular size distances in any cosmology can be found at http://www.astro.ucla.edu/~wright/CosmoCalc.html.

$T_b\,\Delta v\,\Omega_s = I_{CO}\Omega_{s\star b}(1+z)$, where $\Omega_{s\star b}$ is the solid angle of the source convolved with the telescope beam. Then the line luminosity $L'_{CO} = T_b\,\Delta v\,\Omega_s D_A^2 = \Omega_{s\star b} D_L^2 I_{CO}(1+z)^{-3}$, or

$$L'_{CO} = 23.5\,\Omega_{s\star b}\,D_L^2\,I_{CO}\,(1+z)^{-3}, \tag{2}$$

where L'_{CO} is measured in K km s^{-1} pc^2, $\Omega_{s\star b}$ in arcsec^2, D_L in Mpc, and I_{CO} in K km s^{-1}. If the source is much smaller than the beam, then $\Omega_{s\star b} \approx \Omega_b$.

The line luminosity, L'_{CO}, can also be expressed for a source of any size in terms of the total line flux, $L'_{CO} = (c^2/2k)S_{CO}\,\Delta v\,\nu_{obs}^{-2}\,D_L^2\,(1+z)^{-3}$, or

$$L'_{CO} = 3.25\times10^7\,S_{CO}\,\Delta v\,\nu_{obs}^{-2}\,D_L^2\,(1+z)^{-3}. \tag{3}$$

Because L'_{CO} is proportional to brightness temperature, the L'_{CO} ratio for two lines in the same source is equal to the ratio of their intrinsic brightness temperatures averaged over the source. These ratios provide important constraints on physical conditions in the gas. For thermalized optically thick CO emission the intrinsic brightness temperature and line luminosity are independent of J and rest frequency. For example, $L'_{CO}(J = 3\text{–}2) = L'_{CO}(J = 1\text{–}0)$.

By observing CO emission from higher J transitions for high-redshift galaxies researchers can maintain the same approximate observed frequency as redshift increases. Equations 2 and 3 show that for fixed line luminosity (L'_{CO}) and a fixed observed frequency (or a fixed beam size), the observed integrated line intensity and the integrated flux do not scale as the inverse square of luminosity distance (D_L^{-2}), but rather as $(1+z)^3 D_L^{-2}$. This substantial negative K-correction (Solomon, Downes & Radford 1992a,b) is one of the reasons the relatively clear 3-mm atmospheric window, with instruments developed for observation of CO(1–0) in the local Universe, has been the most important wavelength band for observations of CO from EMGs at $z \geq 2$.

A significant fraction of the EMGs are gravitationally imaged by an intervening galaxy. The luminosities L and L' calculated without correction for the magnification by the gravitational lens are, therefore, only apparent luminosities. If a model of the gravitational lens is available, the intrinsic luminosities can be calculated from $L_{int} = L_{app}/\mu$ and $L'_{int} = L'_{app}/\mu$, where μ is the magnification factor of the gravitational lens. Wiklind & Alloin (2002) have reviewed gravitational lensing of EMGs.

2.2. From CO Luminosity to Molecular Mass

Observation of emission from CO rotational transitions is the dominant means of tracing interstellar molecular clouds, which consist almost entirely of molecular hydrogen (H_2). Molecular hydrogen rather than atomic hydrogen is the principal component of all interstellar clouds with density $n > 100$ cm^{-3} owing to a balance between formation on dust and self-shielding of H_2 from photodissociation (Solomon & Wickramasinghe 1969) by the interstellar radiation field. This transition from atomic to molecular hydrogen at a moderate interstellar density

means that all dense clouds are molecular. Molecular clouds are the raw material for star formation and a critical component in the evolution of galaxies. The first generation of stars must have formed, in the absence of heavy elements, from HI with only trace amounts of H_2 available to provide essential cooling. However, the huge IR luminosity seen in ULIRGs and EMGs is clearly emitted by interstellar dust, and we can expect all dense, dusty clouds to be molecular. H_2 has strongly forbidden rotational transitions there, and the H_2 vibration-rotation lines require high temperature to be produced, for example, by UV excitation or shocks. In the absence of these special circumstances, the H_2 is invisible.

CO emission is the best tracer of molecular hydrogen for two reasons. It is a very stable molecule and the most abundant molecule after H_2. Second, a weak dipole moment ($\mu_e = 0.11$ Debye) means that CO rotational levels are excited and thermalized by collisions with H_2 at relatively low densities. Strong CO emission from interstellar gas dominated by H_2 is ubiquitous. The critical density necessary to produce substantial excitation of a rotational transition is given approximately by $n(H_2) \geq A/C$ where A is the Einstein coefficient for spontaneous decay and C is the collisional rate coefficient. The A coefficient scales as $\mu^2\nu^3$ where μ is the dipole moment and $\nu(J, J-1) = 2BJ$ for a simple rotational ladder is the frequency of the transition. In practice, the critical density is lowered by line trapping for CO emission and for emission from other optically thick tracers such as HCN and CS. The full multi-level excitation problem is usually solved using the large velocity gradient (LVG) approximation (Scoville & Solomon 1974, Goldreich & Kwan 1974). The effective density for strong CO emission ranges from $n(H_2) \approx 300$ cm^{-3} for J = (1–0) to $\approx$3000 cm^{-3} for J = (4–3) or (5–4). Of course, the higher J transitions also require a minimum kinetic temperature for collisional excitation. For high-z galaxies there is another obvious requirement. The large quantities of dust and molecular gas observed in EMGs clearly indicate not only ongoing star formation but also substantial enrichment by previous star formation. Researchers have known for some time that many quasar emission line regions show substantial metallicity; EMGs have not only a high metallicity, but also a huge mass of enriched interstellar matter much larger and more extensive than that of a quasar emission line region.

The H_2 mass-to-CO luminosity relation can be expressed as

$$M(H_2) = \alpha L'_{CO}, \tag{4}$$

where $M(H_2)$ is defined to include the mass of He, so that $M(H_2) = M_{gas}$, the total gas mass, for molecular clouds. For the Galaxy, three independent analyses yield the same linear relation between the gas mass and the CO line luminosity: (*a*) correlation of optical extinction with ^{13}CO (Dickman 1978); (*b*) correlation of the flux of γ rays, produced by cosmic ray interactions with protons, with the CO line flux for the Galactic molecular ring (Bloemen et al. 1986, Strong et al. 1988); and (*c*) the observed relations between virial mass and CO line luminosity for Galactic giant molecular clouds (GMCs) (Solomon et al. 1987), corrected for a solar circle radius of 8.5 kpc. All these methods indicate that in our Galaxy,

$\alpha \equiv M_{\rm gas}/L'_{\rm CO} = 4.6\ M_\odot$ (K km s^{-1} pc^2)$^{-1}$ (Solomon & Barrett 1991). (Some authors use X rather than α as a symbol for this conversion factor, even though X by convention relates H_2 column density and line-integrated CO intensity.)

For a single cloud or an ensemble of nonoverlapping clouds, the gas mass determined from the virial theorem, $M_{\rm gas}$, and the CO line luminosity, $L'_{\rm CO}$, are related by

$$M_{\rm gas}/L'_{\rm CO} = \alpha = \left(\frac{4\,m' \times 1.36}{3\,\pi\,G}\right)^{1/2} \frac{n^{1/2}}{T_{\rm b}} \ = \ 2.6\,\frac{n^{1/2}}{T_{\rm b}}, \tag{5}$$

where m' is the mass of an H_2 molecule multiplied by 1.36 to account for He, n (cm^{-3}) is the average H_2 number density in the clouds, and $T_{\rm b}$ (K) is the intrinsic (rest-frame) brightness temperature of the CO line. $M_{\rm gas}$ is in $M_\odot$ and $L'_{\rm CO}$ is in K km s^{-1} pc^2 (Dickman, Snell, & Schloerb 1987; Solomon et al. 1987). This is the physical basis for deriving gas mass from CO luminosity. The existence of gravitationally bound clouds is confirmed by the agreement between α determined from application of the virial theorem, using measured velocity dispersions and sizes for the Milky Way clouds, and α determined from the totally independent methods (*a*) and (*b*) discussed above.

Use of the Milky Way value for the molecular gas mass to CO luminosity ratio, $\alpha = 4.6\ M_\odot$ (K km s^{-1} pc^2)$^{-1}$, overestimates the gas mass in ULIRGs and probably in EMGs. After high-resolution maps were produced for a few ULIRGs (Scoville et al. 1991) it became apparent that the molecular gas mass calculated using the Milky Way value for α was comparable to and in some cases greater than the dynamical mass of the CO-emitting region. This contradiction led to a new model (Downes, Solomon & Radford 1993; Solomon et al. 1997) for CO emission in ULIRGs. Unlike Galactic clouds or gas distributed in the disks of galaxies, most of the CO emission in the centers of ULIRGs may not come from virialized clouds, but from a filled intercloud medium, so the linewidth is determined by the total dynamical mass in the region (gas and stars), that is, $\Delta V^2 = G\,M_{\rm dyn}/R$. The CO luminosity depends on the dynamical mass as well as the gas mass. The CO line emission may trace a medium bound by the total potential of the galactic center, containing a mass $M_{\rm dyn}$ consisting of stars and dense clumps, and an interclump medium containing the CO emitting gas with mass $M_{\rm gas}$.

Defining $f \equiv M_{\rm gas}/M_{\rm dyn}$, the usual CO-to-$H_2$ mass relation becomes (Downes, Solomon & Radford 1993)

$$M_{\rm dyn}/L'_{\rm CO} = f^{-1/2}\alpha = f^{-1/2}\,2.6\,(\bar{n})^{1/2}\,T_{\rm b}^{-1},$$

$$M_{\rm gas}/L'_{\rm CO} = f^{1/2}\alpha = f^{1/2}\,2.6\,(\bar{n})^{1/2}\,T_{\rm b}^{-1},$$

and

$$M_{\rm dyn}M_{\rm gas} = (\alpha L'_{\rm CO})^2, \tag{6}$$

where $\bar{n}$ is the gas density averaged over the whole volume. The quantity $\alpha L'_{\rm CO}$ measures the geometric mean of total mass and gas mass. It underestimates total mass and overestimates gas mass. Hence if the CO emission in ULIRGs comes from regions not confined by self-gravity, but instead from an intercloud medium bound by the potential of the galaxy, or from molecular gas in pressure, rather than gravitational equilibrium, then the usual relation $M_{\rm gas}/L'_{\rm CO} = \alpha$ must be changed. The effective α is lower than $2.6n^{1/2}/T_{\rm b}$.

Extensive high-resolution mapping of CO emission from ULIRGs shows that the molecular gas is in rotating disks or rings. Kinematic models (Downes & Solomon 1998) in which most of the CO flux comes from a moderate density warm intercloud medium have been used to account for the rotation curves, density distribution, size, turbulent velocity, and mass of these molecular rings. Gas masses were derived from a model of radiative transfer rather than the use of a standard conversion factor. The models yield gas masses of $\sim 5 \times 10^9\ M_\odot$, approximately five times lower than the standard method, and a ratio $M_{\rm gas}/L'_{\rm CO} \approx 0.8\ M_\odot$ (K km s^{-1} pc^2)$^{-1}$. The ratio of gas to dynamical mass $M_{\rm gas}/M_{\rm dyn} \approx 1/6$ and a maximum ratio of gas to total mass surface density $\mu/\mu_{\rm tot} = 1/3$. This effective conversion factor $\alpha = 0.8\ M_\odot$ (K km s^{-1} pc^2)$^{-1}$ for ULIRGs has been adopted for EMGs by many observers of high-z CO emission and we use it throughout this review. However, until a significant number of EMGs are observed with sufficient angular resolution to enable a calibration of α, the extrapolation in the use of $\alpha = 0.8$ to EMGs from ULIRGs must be regarded as tentative.

2.3. Classification of the EMGs

The list of 36 EMGs reported in the literature at the time of this review is given in Table 1, together with their derived properties. The gas masses listed were calculated using the luminosity of the lowest available CO transition and $\alpha = 0.8$ (see Section 2.2). All quantities assume the cosmology adopted for this review. Appendices 1, 2, and 3 list the observed properties from which the quantities in Table 1 were calculated.[2] The overwhelming majority of these detections were made with

[2]Appendix 1 lists coordinates, redshift, galaxy type, and magnification for each EMG. Appendix 2 gives velocity-integrated flux densities ($S\Delta v$), linewidths full-width at half-maximum (FWHM) (Δv), peak line flux densities (S), line luminosities (L') for the CO transitions observed in the EMGs, and inferred molecular gas masses. The observed quantities listed are those reported in the references cited, after adjustment for the cosmology assumed in this review. Where lens models exist, intrinsic luminosities are listed, calculated using the magnifications given in Appendix 1. In addition to CO, data for detections of HCN are listed, as well as for CI whose fine-structure lines originate from interstellar molecular gas. Appendix 3 gives the observed continuum flux densities at various wavelengths of the EMGs, together with the inferred FIR luminosity, including the intrinsic luminosity where it is possible to correct for lens magnification. Brackets indicate the measurements that were included in the calculation of the listed luminosity values cited. Frequently, only a single measurement was used to estimate the luminosity, together with a set of assumptions, so the values listed should be regarded with caution.

TABLE 1 EMG properties: line and FIR luminosities, gas and dust masses, star formation rate

EMG	Redshift z	Transition	L'(app.) ($10^{10}\ L'_*$)[a]	$L_{\rm FIR}$(app.) ($10^{12}\ L_\odot$)	Lens magnification	L'(int.) ($10^{10}\ L'_*$)[a]	$L_{\rm FIR}$(int.) ($10^{12}\ L_\odot$)	$M_{\rm gas}$ ($10^{10}\ M_\odot$)	$M_{\rm dust}$ ($10^{8}\ M_\odot$)	SFR ($M_\odot$ year^{-1})	$\tau_{\rm sf}$ (10^6 years)
SMM J02396	1.062	CO(2–1)	5.1 ± 0.5	16.3	2.5	2.0	6.5	1.6		975	16
Q0957+561	1.414	CO(2–1)	0.9 ± 0.5	14	1.6	0.6	6	0.4	2.5	900	4
HR10	1.439	CO(1–0)	6.5 ± 1.1	6.5	?	—	—	$5.2\,\mu^{-1}$	$6.8\,\mu^{-1}$		
IRAS F10214	2.286	CO(3–2)	11.3 ± 1.7	60	17	0.7	3.6	0.6		540	11
SMM J16371	2.380	CO(3–2)	3.0 ± 0.6	—	?	—	—	$2.4\,\mu^{-1}$			
SMM J16368	2.385	CO(3–2)	6.9 ± 0.6	16	?	—	—	$5.5\,\mu^{-1}$			
53W002	2.393	CO(3–2)	3.6 ± 0.4	—	1	3.6	—	2.9			
SMM J16366	2.450	CO(3–2)	5.6 ± 0.9	20	?	—	—	$4.5\,\mu^{-1}$			
SMM J04431	2.509	CO(3–2)	4.5 ± 0.6	13	4.4	1.0	3	0.8		450	18
SMM J16359	2.517	CO(3–2)	18.9 ± 0.8	45	45	0.4	1	0.3	2	150	20
Cloverleaf	2.558	CO(3–2)	44 ± 1	59	11	4.0	5.4	3.2	1.5	810	40
SMM J14011	2.565	CO(3–2)	9.4 ± 1.0	20	5–25	0.4–1.9	0.8–4.0	0.3–1.5	0.13–0.65	120–600	25
VCV J1409	2.583	CO(3–2)	7.9 ± 0.7	35	?	—	—	$6.3\,\mu^{-1}$	$38\,\mu^{-1}$		
LBQS 0018	2.620	CO(3–2)	5.4 ± 0.9	33	?	—		$4.3\,\mu^{-1}$			
MG0414	2.639	CO(3–2)	9.2	32	?	—		$7.4\,\mu^{-1}$			
MS1512-cB58	2.727	CO(3–2)	1.4 ± 0.3	3.1	32	0.043	0.1	0.03		15	20
LBQS 1230	2.741	CO(3–2)	3.0 ± 1.0	36	?	—	—	$2.4\,\mu^{-1}$	$11\,\mu^{-1}$		
RX J0911.4	2.796	CO(3–2)	11.3 ± 4.3	51	22	0.52	2.3	0.4		345	12
SMM J02399	2.808	CO(3–2)	12.2 ± 1.6	11	2.5	4.9	4.4	3.9	6–8	660	59
SMM J04135	2.846	CO(3–2)	22 ± 5	31	1.3	17	24	13.0	18	3600	36
B3 J2330	3.092	CO(4–3)	3.4 ± 0.8	28	1	3.4	28	2.7		1950	14
SMM J22174	3.099	CO(3–2)	3.7 ± 0.9	12	?	—		3.0		1800	17

MG0751	3.200	CO(4–3)	16 ± 1	49	17	1.0	2.9	0.8		435	18
SMM J09431	3.346	CO(4–3)	3.2 ± 0.3	20	1.2	2.7	12	2.2		1800	12
SMM J13120	3.408	CO(4–3)	5.2 ± 0.9	12	?	—		$4.2\,\mu^{-1}$			
TN J0121	3.520	CO(4–3)	5.4 ± 1.0	7	1	5.4	7	4.3		1050	41
6C1908	3.532	CO(4–3)	5.2 ± 1.0	9.8	1	5.2	9.8	4.2		1470	29
4C60.07b	3.791	CO(1–0)	8.7 ± 1.7	13	1	8.7	13	7.0		1950	36
4C60.07n	3.791	CO(1–0)	5.2 ± 0.6		1	5.2		4.2			
4C60.07b		CO(4–3)	6.0 ± 0.9		1	6.0					
4C60.07n		CO(4–3)	3.0 ± 0.2		1	3.0					
4C41.17R	3.796	CO(4–3)	4.3 ± 0.5	20	1	4.3	20	3.4	4.6	3000	11
4C41.17B	3.796	CO(4–3)	2.2 ± 0.5		1	2.2		1.8			
APM 08279	3.911	CO(1–0)	9.1 ± 2.7	200	7	1.3	29	1.0	5.8	4350	2
PSS J2322	4.119	CO(1–0)	12 ± 5	23	2.5	5.0	9.3	4.0		1800	22
BRI 1335N	4.407	CO(2–1)	3.3 ± 1.1		?	—	—	$2.6\,\mu^{-1}$			
BRI 1335S	4.407	CO(2–1)	4.8 ± 1.1		?	—	—	$3.8\,\mu^{-1}$			
BRI 1335		CO(5–4)	8.2 ± 0.9	28	?	—	—		$17\,\mu^{-1}$		
BRI 0952	4.434	CO(5–4)	2.8 ± 0.3	9.6	4	0.7	2.4	0.5	0.7	360	19
BR 1202N	4.692	CO(2–1)	5.2 ± 1.0		?	—		7			
BR 1202S	4.695	CO(2–1)	4.6 ± 0.8		?	—					
BR 1202		CO(4–3)	7.6 ± 1.5	71	?	—	—		$19\,\mu^{-1}$		
TN J0924	5.203	CO(1–0)	8.2 ± 1.6		1	8.2		6.6			
SDSS J1148	6.419	CO(3–2)	2.6 ± 0.6	27	?	—	—	2.1	$2.4\,\mu^{-1}$		

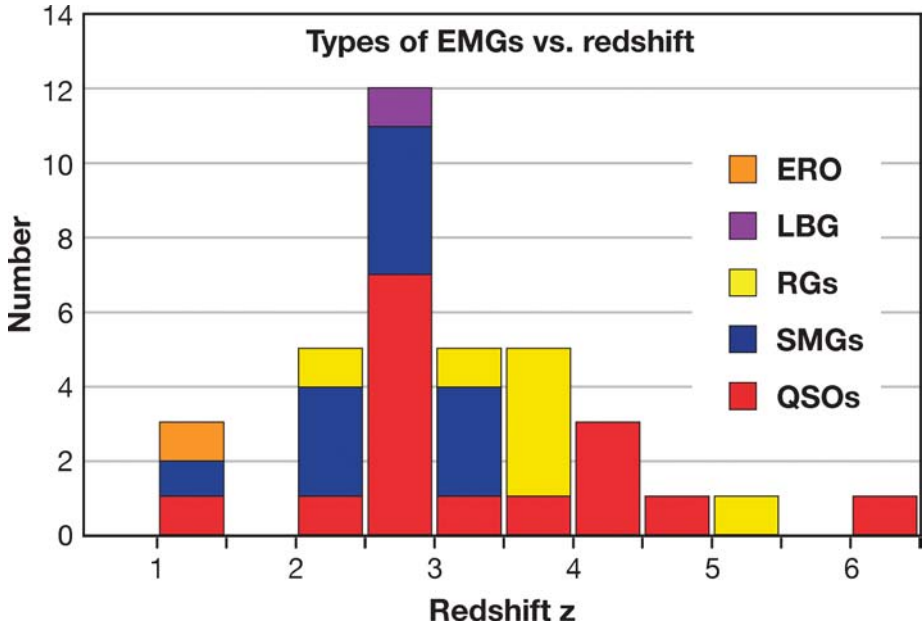

Figure 1 Distribution in redshift of the 36 known EMGs: 16 quasi-stellar objects (QSO), 11 submillimeter galaxies (SMG), 7 radio galaxies (RG), one Lyman break galaxy (LBG), and one extremely red object (ERO). Despite the large selection effects of the flux-limited sample, the distribution broadly reflects the current understanding of when most of the star formation in the Universe is thought to have occured.

the IRAM interferometer. Lists of EMGs have been published by Cox et al. (2002), Carilli et al. (2004), Hainline et al. (2004), and Beelen (http://www.astro/nni-bonn.di/∼beelen/database.xml). The sources are listed in all tables and appendices in order of redshift. No blind survey for high-z CO emission has been done because of its prohibitive cost in observing time with present instruments. Were such a blind survey to be done eventually by the Atacama Large Millimeter Array (ALMA), it could result in additional types of EMGs. Figure 1 shows the number of EMGs by type as a function of redshift. Despite the selection effects that attend the detection of EMGs, one can see that the current largely flux-limited sample broadly reflects the epoch where most star formation in the Universe is currently thought to occur.

With recent improvements in millimeter bolometers, large numbers of quasi-stellar objects (QSOs) have been observed in 1.2-mm continuum emission. Approximately 30% of the bright QSOs at all redshifts $z > 2$ are strong millimeter/submillimeter continuum emitters with a typical inferred rest-frame luminosity of $L_{\rm FIR} \sim 10^{13}\ L_{\odot}$ (Izaak et al. 2002, Omont et al. 1996a). The percentage of submillimeter detections is higher (60%) for gravitationally lensed quasars (Barvainis & Ivison 2002). Identifying the redshift appropriate for a CO emission search can be difficult because the molecular gas in the host galaxy may have a significantly

different redshift from the broad optical emission line region of the QSO. A key question for the EMGs identified with QSOs is whether the FIR luminosity is powered by rapid star formation (starbursts) in the molecular clouds or by the active galactic nucleus (AGN) that may be accreting molecular gas.

In SMGs, unlike the optically selected quasars, the total luminosity is completely dominated by their (rest-frame) FIR emission. The surveys at 850 μm, primarily carried out with the Submillimeter Common-User Bolometer Array (SCUBA) instrument, on the James Clerk Maxwell Telescope (JCMT), have found several hundred galaxies, or about 1 arcmin^{-1} (see, for example, Scott et al. 2002). They represent a substantial part of the FIR background and may contribute as much as half of all star formation at high z. Although many SCUBA galaxies harbor AGNs, the AGNs contribute only a small fraction of the bolometric luminosity, which is dominated by star formation (Alexander et al. 2004). Only a small subset of about 15 blank-field submillimeter sources have been observed in CO emission.

A relatively small proportion (19%) of EMGs are identified with radio galaxies. Radio galaxies are a rare population and are not selected for being gravitationally lensed. However, seven IR-luminous radio galaxies have been observed in CO emission, and these include some of the more interesting examples.

The identification of a set of EMGs with LBGs would be significant in that it would tie the EMGs to a huge population of early Universe objects. However, only a single LBG has been detected in CO emission (Baker et al. 2004). The low CO line luminosity of this object compared with the other EMGs suggests that LBGs form a different class of early Universe galaxies, something that remains to be confirmed using ALMA.

2.4. Examples of EMGs

This section presents and discusses EMGs by type and historically within each type.

2.4.1. IRAS F10214 In 1991, IRAS FSC10214 + 4724 was shown to be an extraordinarily luminous high-redshift IR source (Rowan-Robinson et al. 1991). With a redshift of $z = 2.3$ it was by far the most luminous IR galaxy yet found, more than 30 times as luminous as local ULIRGs. Shortly after IRAS F10214 was identified, the first high-z CO emission was searched for and found in the (3–2), (4–3), and (6–5) lines (Brown & Vanden Bout 1991, 1992; Solomon, Downes & Radford 1992a). Allowing for the negative K-correction, Solomon, Downes & Radford (1992b) found the CO line luminosity, $L'_{\rm CO}$, calculated from the flux measured at the IRAM 30-m Telescope, to be 100 times less than first estimated, but still about one order of magnitude greater than that in any galaxy in the local Universe, yielding a molecular gas mass of 10^{11} $M_\odot$, equal to the baryonic mass of an entire large galaxy. [Agreement between the 12-m and 30-m measured fluxes was obtained with new observations at the 12-m by Radford et al. (1996)]. The strong CO(6–5) line, originating from a rotational level 116 K above the ground

state, and the (6–5)/(3–2) line ratio indicate the presence of moderately dense gas substantially warmer than most of the molecular mass in the Milky Way GMCs or normal spiral galaxies.

Optical and near-IR spectroscopies show both narrow and broad emission line systems, with the narrow lines indicating a Seyfert 2 nucleus (Lawrence et al. 1993) and the broad lines observed in polarized light indicating the presence of an obscured quasar (Goodrich et al. 1996).

High-resolution optical and near-IR imaging (Broadhurst & Leh'ar 1995, Graham & Liu 1995, Matthews et al. 1994) clearly show that F10214 is gravitationally lensed. The 2.2-μm image shows a compact 0.7″ diameter source superposed on a weaker 1.5″ arc. CO maps of the (6–5) line with the IRAM interferometer show an elongated structure that was modeled as a CO arc convolved with the interferometer beam and fit to the CO data (Downes, Solomon & Radford 1995). From the length of the CO arc, the apparent CO luminosity, the linewidth, and the intrinsic brightness temperature of the line (deduced from line ratios), Downes, Solomon & Radford (1995) derived a magnification $\mu = 10 f_{\rm v}$, where $f_{\rm v}$ is the velocity filling factor, or fraction of the full line width intercepted by a typical line of sight. This magnification reduced the intrinsic CO line luminosity and molecular mass to that of local ULIRGs. The radius of the molecular ring was found to be $600/f_{\rm v}$ pc, much larger than that in the AGN torus and similar to that in ULIRGs, but much less than that in a full galactic disk. The magnification for the FIR radiation was 13, and for the mid-IR it was 50.

Recent improved high-resolution maps of CO(3–2), CO(6–5), and CO(7–6) (D Downes & PM Solomon, manuscript in preparation) show that the size of the lensed CO image is $1.6'' \times \leq 0.3''$ ($2.7 \times \leq 0.5$ kpc). More importantly, a velocity gradient is observed along the arc, and line profiles show two distinct kinematic components at the east and west sides, demonstrating that the molecular emission originates in a rotating disk around the quasar. Positions, sizes, and linewidths are the same in all three lines, indicating that they originate in the same volume with the same kinematic distribution. The line ratios indicate a mean emission-weighted kinetic temperature of 50 K and a mean H_2 density of 3000 cm^{-3}. A search for ^{13}CO emission yields a ratio of ^{12}CO/^{13}CO $\geq$ 21, which is similar to high values found in ULIRGs but higher than those of nearby spiral galaxies, indicating a modest opacity for ^{12}CO. The true size of the molecular ring, the CO luminosity, molecular mass, and the excitation of the CO ladder all look similar to those observed in local ULIRGs.

Vanden Bout, Solomon & Maddalena (2004) observed strong HCN(1–0) emmision from F10214 with an intrinsic line luminosity similar to that in local ULIRGs such as Mrk 231 and Arp 220. HCN emission traces dense gas generally associated with the star-forming cores of GMCs (see Section 3.1). The very high ratio of HCN to CO luminosities $L'_{\rm CO}/L'_{\rm HCN} = 0.18$ is characteristic of starbursts in the local Universe. All galaxies with global HCN/CO luminosity ratios greater than 0.07 were found to be luminous ($L_{\rm FIR} > 10^{11}\ L_\odot$) starbursts by Gao & Solomon (2004). F10214 contains both a dust-enshrouded quasar responsible for the mid-IR

luminosity and a much larger molecular ring starburst responsible for a substantial fraction of the FIR luminosity.

2.4.2. CLOVERLEAF Hazard et al. (1984) found the quasar H1413 + 1143 (better known as the Cloverleaf), a broad absorption line QSO at a redshift of $z = 2.55$. It was subsequently identified optically as a lensed object with four bright image components (Magain et al. 1988). Barvainis, Antonucci & Coleman (1992) discovered strong FIR and submillimeter radiation from the Cloverleaf, indicating a substantial dust component with an FIR spectral energy distribution (SED) similar to that of IRAS F10214. This was the first indication that some bright optical high-z quasars also are extremely IR luminous.

Redshifted strong CO(3–2) emission was observed using both the IRAM 30-m Telescope and Plateau de Bure Interferometer (Barvainis et al. 1994), with an apparent line luminosity about three times greater than that from F10214. Barvainis et al. (1997) observed three additional rotational lines (4–3), (5–4), and (7–6) at the IRAM 30-m Telescope and used their line ratios to constrain the physical conditions of the gas and the CO to H_2 conversion factor. These measurements showed $L'_{CO}(4–3) > L'_{CO}(3–2)$, indicating a high kinetic temperature and low optical depths. More recent measurements (Weiß et al. 2003) show a higher (3–2) flux and a lower line ratio (4–3)/(3–2) indicative of lower kinetic temperatures and subthermal excitation. The Cloverleaf CO emission lines have a higher flux density than do the lines from any other high-z source, owing to both powerful intrinsic line luminosities and magnification. As a result, they can be successfully imaged at high angular resolution. The lensing also magnifies the scale of the emission, making it possible to deduce true source size at scales below the instrumental resolution.

Using the millimeter array at the Owens Valley Radio Observatory (OVRO), Yun et al. (1997) obtained an interferometric map of the Cloverleaf in which the CO(7–6) emission was partially resolved. They used *Hubble Space Telescope* (HST) images to model a lens with an elliptical potential and an external sheer. This model constrained the intrinsic size of the CO(7–6) source, which has a radius of approximately 1100 pc. Separation of the red and blue line wings showed a kinematic structure consistent with a rotating disk. Alloin et al. (1997) obtained a high-resolution map (0.5″) with the IRAM interferometer that clearly resolved the emission into four spots similar to the lensed optical radiation. Figure 2 shows an image of the CO(7–6) emission constructed by Venturini and Solomon (2004) from their data. A model based on optical *Hubble Space Telescope* (HST) and radio Very Large Array (VLA) images gave an upper limit to the source radius of approximately 1200 pc. Kneib et al. (1998) used enhanced IRAM CO(7–6) images and HST images to construct two lens models using a truncated elliptical mass distribution with an external shear (galaxy + cluster). From the separation of the kinematic components and the HST-based lens model they deduced a CO radius of only 100 pc and a magnification of 30. This size scale is characteristic of an AGN torus.

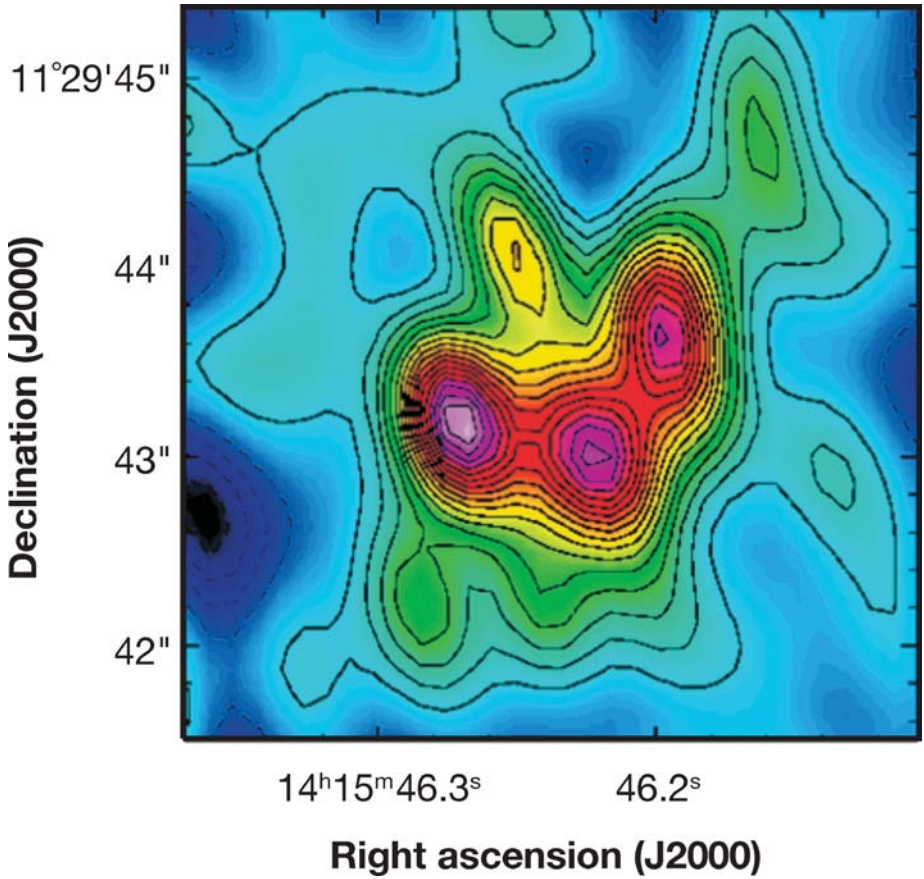

Figure 2 Image of the Cloverleaf in CO(7–6) emission taken with the IRAM interferometer (Alloin et al. 1997). The high observing frequency of 226 GHz provides the angular resolution (0.5″) needed to construct a gravitational lens model based on CO data.

Venturini & Solomon (2003) fit a two-galaxy lensing model directly to the IRAM CO(7–6) map rather than to the optical HST image. The fit obtained by minimizing the difference between the map produced by the lensed model and the IRAM CO(7–6) image yielded a source with disklike structure and a characteristic radius of 800 pc, a value similar to that of the CO-emitting regions present in nearby starburst ULIRGs. The model reproduces the geometry as well as the brightness of the four images of the lensed quasar. The large size of the CO source seems to rule out a scenario in which the molecular gas is concentrated in a very small region around the central AGN. With the magnification of 11 found from this model and the CO(3–2) flux given by Weiß et al. (2003), the total molecular mass is $3.2 \times 10^{10}\ M_{\odot}$, with a molecular surface density of $10^4\ M_{\odot}\ \mathrm{pc}^{-2}$. Weiß et al. (2003) argue that using L'_{CO}(3–2) rather than L'_{CO}(1–0) has only a 10% effect on the

calculated molecular mass. The dynamical mass of the rotating disk is $M_{\rm dyn} \sin^2 i = 2.5 \times 10^{10}\ M_\odot$.

HCN emission traces dense gas generally associated with the star-forming cores of GMCs. Strong HCN(1–0) emission has been observed from the Cloverleaf (Solomon et al. 2003) with an intrinsic line luminosity slightly higher than that in local ULIRGs, such as Mrk 231 and Arp 220, and 100 times greater than that of the Milky Way. To put this in perspective, the intrinsic HCN luminosity of the Cloverleaf is 10 times greater than the CO luminosity of the Milky Way, indicating the presence of $10^{10}\ M_\odot$ of dense star-forming molecular gas.

The molecular and IR luminosities for the Cloverleaf show that the large mass of dense molecular gas indicated by the HCN luminosity could account for a substantial fraction (from star formation), but not all, of the IR luminosity from this quasar. If Arp 220 is used as a standard for the luminosity ratio $L_{\rm FIR}/L'_{\rm HCN}$, then star formation in the dense molecular gas could account for $5 \times 10^{12}\ L_\odot$, or about 20% of the total intrinsic IR luminosity. Using the highest ratio for an ULIRG gives an upper limit of 40%.

The model by Weiß et al. (2003) of the IR spectral energy distribution of the Cloverleaf has two distinct components: one with a warm dust temperature $T_{\rm d} = 115$ K responsible for the mid-IR, and the other much more massive component with $T_{\rm d} = 50$ K that produces the FIR. The model FIR luminosity, 22% of the total, may correspond to the luminosity generated by star formation and the mid-IR to heating by the AGN. Using the model of $L_{\rm FIR}$ yields $L_{\rm FIR}/L'_{\rm HCN} = 1700$, comparable to that of ULIRGs and only a factor of 2 higher than that for normal spiral galaxies (Gao & Solomon 2004). The star formation rate per solar mass of dense gas is then similar to that in ULIRGs and only slightly higher than that in normal spirals.

2.4.3. VCV J1409 + 5628 This EMG is an optically luminous radio-quiet quasar with the strongest 1.2-mm flux density found in the survey by Omont et al. (2003). It has been observed in both CO(3–2) and CO(7–6) emission (Beelen et al. 2004). The line luminosity of $L'_{\rm CO}({\rm app.}) = (7.9 \pm 0.7) \times 10^{10}$ K km s^{-1} pc^2 leads to a gas mass of $M_{\rm gas} = 6.3 \times 10^{10}\, \mu^{-1}\ M_\odot$, which is ∼20% of $M_{\rm dyn}$ for reasonable inclinations. If the extent of the radio continuum, from a VLA image at 1.4 GHz, represents the extent of the CO emission, the molecular gas is confined to a torus or disk of diameter 1–5 kpc. This is similar both to the molecular gas extents inferred from lens models of F10214 and the Cloverleaf and to what is observed in ULIRGs.

2.4.4. PSS J2322 + 1944 This EMG is an IR-luminous quasar. The extent of its molecular gas has been inferred from a remarkable gravitationally lensed image of the CO emission—a so-called Einstein Ring. Carilli et al. (2003) studied this lensed system on subkiloparsec scales with the 0.6″ resolution of the VLA at 43 GHz, where the CO(2–1) line from this $z = 4.12$ object is redshifted. The VLA image is shown in Figure 3. The data are consistent with a dynamical mass of $M_{\rm dyn} = 3 \times 10^{10} \sin^{-2} i\ M_\odot$ and confinement of the molecular gas in a disk

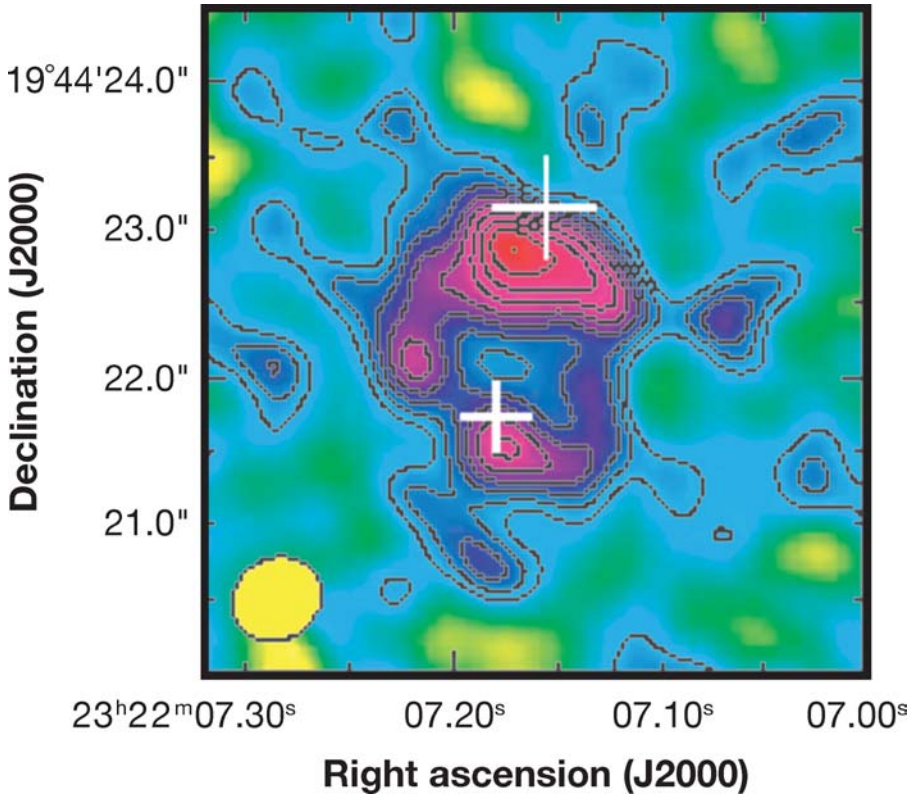

Figure 3 The Einstein Ring in PSS2322, observed in CO(2–1) emission using the VLA at a resolution of 0.6″ (Carilli et al. 2003).

of diameter 2.2 kpc. The radio continuum is co-spatial with the molecular gas, and the star formation rate is ∼900 $M_\odot$ year^{-1}. PSS J2322 + 1944 is the fourth EMG to be observed in [CI] emission. This object provides strong evidence for the presence of active star formation in the host galaxy of a luminous high-redshift quasar.

2.4.5. BR 1202-0725 This is an optically bright radio-quiet quasar, the third EMG to be discovered (Omont et al. 1996b), and the first to show multiple components. Whether these two components, separated by 4″, are companion objects or the result of gravitational lensing remains an issue. High-resolution imaging (Carilli et al. 2002a) using the VLA of the CO(2–1) emission has shown that the southern component is roughly twice as massive as the northern component, and there is a significant difference in the velocity widths of the CO lines of the two components. This finding provides evidence against the presence of a gravitational lens. However, the total molecular gas mass exceeds the dynamical mass of the system

unless an unreasonably low value of α is used to calculate $M_{\rm gas}$. Magnification by a gravitational lens would allow for more reasonable values of α.

2.4.6. APM 08279 + 5245 This extremely luminous broad absorption line quasar was accidentally discovered in a survey for cool carbon stars (Irwin et al. 1998). The high redshift of $z = 3.9$ would have made it the most luminous known object in the Universe were it not for the magnification of a gravitational lens (Egami et al. 2000). The magnification at optical wavelengths can be as large as $\mu = 100$; for CO emission it is much less, $\mu = 7$ (Downes et al. 1999, Lewis et al. 2002). The CO(4–3) and (9–8) emissions were first observed in APM 08279 with the IRAM interferometer (Downes et al. 1999). The strong (9–8) emission indicates the presence of hot dense gas with a kinetic temperature of approximately 200 K. The observed ratio of $L_{\rm FIR}/L'_{\rm CO}$ is twice that of other EMGs. In addition to the central molecular emission region, observed in four CO transitions, high-resolution images of the CO(2–1) emission with the VLA reveal two emission regions lying to the north and northeast, 2–3″ distant from the central region (Papadopoulos et al. 2001). If real, these could be companion galaxies. The nuclear CO(1–0) emission is imaged in a (partial) Einstein Ring (Lewis et al. 2002).

2.4.7. SDSS J1428 + 5251 This is the most distant known quasar, with a redshift of $z = 6.42$. It was shown to be an EMG via the observations of CO(3–2) emission using the VLA, and CO(6–5) and CO(7–6) emissions using the IRAM interferometer (Bertoldi et al. 2003b, Walter et al. 2003). The CO observations imply a mass of molecular gas $M_{\rm gas} = 2.1\times10^{10}\mu^{-1}\,M_\odot$. The thermal dust emission (Bertoldi et al. 2003a) leads to a star formation rate of $\sim$3000 $M_\odot$ year^{-1}. This is clear evidence for the presence of vast amounts of molecular gas, composed of heavy elements, only $\sim$850 million years following the Big Bang. High-resolution ($0.17'' \times 0.13''$; $\leq$1 kpc) imaging of the CO(3–2) emission using the VLA (Walter et al. 2004), shown in Figure 4, suggests that this source may be a merger of two galaxies.

2.4.8. SMM J02399 − 0136 This SMG was the first SCUBA source identified as an EMG (Frayer et al. 1999) using OVRO. It is the brightest galaxy detected in an early SCUBA survey of rich lensing clusters (Smail, Ivison & Blain 1997). J02399 harbors an AGN (Ivison et al. 1998). The observed integrated line strength of the CO(3–2) line, with the observed CO redshift of $z = 2.808$, leads to $L'_{\rm CO}$(app.) = 12×10^{10} K km s^{-1} pc^2. Correction for a cluster lens magnification of $\mu = 2.5$ yields $L'_{\rm CO}$(int.) = 4.9×10^{10} K km s^{-1} pc^2. This is comparable to CO luminosities for ULIRGs and was the first evidence that SCUBA sources identified as EMGs were similar in nature to ULIRGs. Higher-resolution observations of the CO emission at IRAM confirmed the OVRO detection (Genzel et al. 2003). These data were fitted to a rotating disk model very similar to but larger in size than that seen in ULIRGs: a molecular gas mass $M_{\rm gas} = 3.9 \times 10^{10}\,M_\odot$ confined within a radius of 8 kpc. This source remains one of few EMGs with the potential for molecular gas to be extended in a disk with radius larger than 2 kpc.

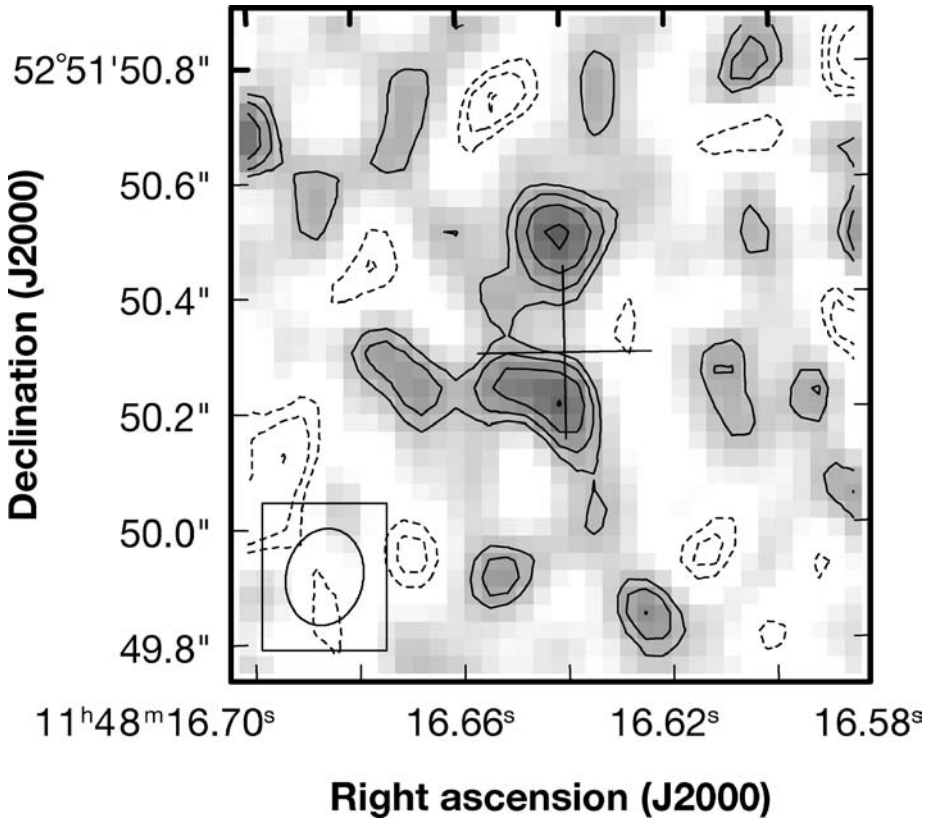

Figure 4 SDSS J1148, a quasar at $z = 6.4$ imaged in CO(3–2) emission using the VLA at a resolution of $0.17'' \times 0.13''$ (Walter et al. 2004). This system is a possible merger of two components that resemble the ULIRGs of the more local Universe. The presence of CO in this system is evidence for substantial enrichment in heavy metals ∼850 million years after the Big Bang.

2.4.9. SMM J14011 + 0252 This SMG was the second SCUBA source from the Lensing Cluster Survey (Smail, Ivison & Blain 1997) to be detected in CO emission; it has been heavily observed since being identified as an EMG. There is no evidence for the presence of an AGN in J14011. The detection of CO(3–2) emission (Frayer et al. 1999) at OVRO was followed by more interferometry to determine the location of the CO source among the 850-μm peaks in the SCUBA image and its extent. From combined OVRO and Berkeley-Illinois-Maryland Association (BIMA) observations Ivison et al. (2001) argued that the CO emission was extended on a scale of diameter 20 kpc, assuming a cluster magnification of $\mu = 2.5$, well beyond what is seen in ULRIGs. Higher signal-to-noise observations at IRAM (Downes & Solomon 2003) did not confirm this extent, as the CO emission is confined to an observed disk of only $2.2''$, or a <7 kpc for $\mu \geq 2.5$.

2.4.10. SMM J16359 + 6612 This is a somewhat lower luminosity ($L_{\rm FIR} = 10^{12}\ L_\odot$) SMG that nevertheless has been observed in the CO(3–2) emission aided by a gravitational lens that provides a total magnification factor of $\mu = 45$. The image obtained with the IRAM interferometer (Kneib et al. 2004a), together with spectra of the three image components, is shown in Figure 5. CO observations of SMM J16359 have also been reported by Sheth et al. (2004). This is the third SMG reported to have spatially resolved CO emission. Here, the quality of the data together with the lens model of Kneib et al. (2004b) leads to an inferred disk size of 3×1.5 kpc. Whereas the FIR luminosity is comparable to that of Arp 220, the CO luminosity is approximately half that of Arp 220. The mass inferred from the CO luminosity is 30% or 60% of the calculated dynamical mass for a ring-disk structure or a merger, respectively.

2.4.11. 4C41.17 This is one of only seven radio galaxies to be observed in CO emission. High-z radio galaxies (HzRGs) have been difficult to detect in CO emission because the candidates searched are not gravitationally lensed and the observed peak CO flux densities are small ($\sim$2 mJy). Stevens et al. (2003) have argued that HzRGs and their companions, revealed in deep 850-μm images, form central cluster ellipticals. Four of the seven HzRG examples cited by Stevens et al. (2003), including 4C41.17, are also EMGs. A position-velocity plot of the CO(4–3) emission (De Breuck et al. 2004) clearly reveals two components. Both are gas-rich systems, each with $M_{\rm gas} \sim 3 \times 10^{10}\ M_\odot$. Their velocity separation leads to a dynamical mass $M_{\rm dyn} \sim 6 \times 10^{11} \sin^{-2} i\ M_\odot$, for the potential binding of the components. The system could be two gas-rich galaxies merging to form a massive cD elliptical galaxy.

3. DISCUSSION

3.1. Molecular Gas Mass and Star Formation Efficiency

The intrinsic line luminosities given in Table 1 have been corrected for magnification for those sources with known lensing and published estimates of the magnification. For sources without apparent lensing we have adopted the measured line luminosity (assumed the magnification $\mu = 1$) in the figures and discussion of this section. The CO line luminosity of EMGs covers a wide range of $L'_{\rm CO} = (3\text{–}160) \times 10^9$ K km s^{-1} pc^2. Not surprisingly, because this is basically a flux-limited sample, the lowest line luminosities occur for sources (primarily QSOs) with high magnification. The average CO line luminosity is $\langle \log(L'_{\rm CO}) \rangle = 10.45 \pm 0.47$ corresponding to an average gas mass of $2.3 \times 10^{10}\ M_\odot$ using $\alpha = 0.8$. There is little difference between the average CO luminosities among the three categories of sources QSOs, SMGs, and radio galaxies.

Figure 6 shows the CO line luminosity (for the lowest J transition for which data exist) as a function of redshift for EMGs and samples of ULIRGs, LIRGs

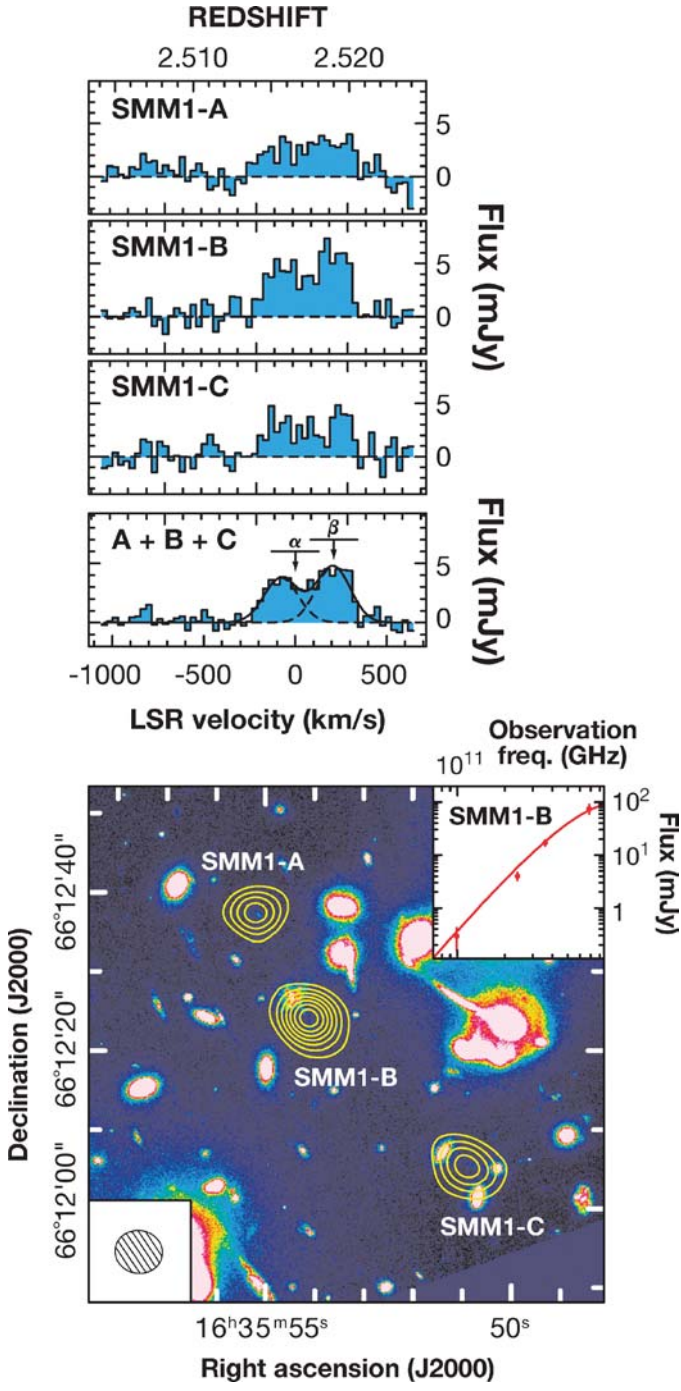

(luminous IR galaxies), and normal spirals. In comparison with EMGs the average line luminosity for ULIRGs in the local Universe is smaller by about a factor of 3 and with a much smaller range, $\log(L'_{\rm CO}) = 9.98 \pm 0.13$ (Solomon et al. 1997). However, there is significant overlap between CO luminosities from these high-z galaxies and those in the local Universe, including ULIRGs, luminous IR galaxies (LIRGs), and even some normal spirals. For example, the ULIRG 20087-0308 has a CO line luminosity of 1.8×10^{10} K km s^{-1} pc^2, larger than that of approximately one third of EMGs. Local interacting galaxies with much more modest IR luminosities such as Arp 302 also have CO luminosities close to the midrange found in EMGs. The normal, isolated spiral NGC3147 has a CO luminosity of 0.7×10^{10} K km s^{-1} pc^2, larger than six times that of EMGs. Most normal, large spiral galaxies have a CO luminosity approximately a factor of 5–10 times less than that of ULIRGs and 10–30 times less than that of EMGs.

Assuming a constant conversion factor, EMGs have, on average, a higher molecular gas mass than the most gas-rich local Universe galaxies, but only a few times higher. In the local Universe there appears to be a "ceiling" for ULIRGs with $M_{\rm gas} < 2 \times 10^{10}\ M_\odot$. Approximately two thirds of the EMGs lie above this local maximum, with a typical gas mass of $5 \times 10^{10}\ M_\odot$ (approximately 30 times the molecular mass of the Milky Way). This difference between local and high-redshift gas masses may be important in understanding the nature of the high-z galaxies and early galaxy evolution. One possibility is that EMGs have the same molecular gas mass as do ULIRGs but have a lower CO to H_2 conversion factor. Or, they may have the same conversion factor and thus contain more molecular mass, possibly distributed over a larger disk. We assume the conversion factor is the same here and in the following sections.

The ratio of FIR luminosity to CO luminosity, $L_{\rm FIR}/L'_{\rm CO}$, is an indicator of the star formation rate per solar mass of molecular gas and is often taken as a measure of the star formation efficiency (Young et al. 1986, Solomon & Sage 1988). Figure 7 shows this ratio as a function of redshift. The star formation efficiency for the EMGs at high z is similar to or slightly higher than that for ULIRGs in the local Universe with an (logarithmic) average $L_{\rm FIR}/L'_{\rm CO} = 350$; this translates into a star formation efficiency of $L_{\rm FIR}/M_{\rm gas} = 430\ L_\odot/M_\odot$.

←

Figure 5 The *lower panel* shows SMM J16359 in CO(3–2) emission that has been triply imaged by a gravitational lens (Kneib et al. 2004a). The total magnification by the lens is $\mu = 45$, making this observation of CO in a somewhat less luminous SMG possible. The CO contours are superimposed on an HST image of Abell 2218 and show good registration with their optical counterparts. The synthesized CO beam ($\sim 6''$) is shown in the *lower left corner*. The SED in the range 450–3000 μm is shown in the *upper right corner* (Kneib 2004b). The *upper panel* shows the CO spectra from each image together with the combined spectrum. The redshifts deduced from HST imaging and Hα spectroscopy, shown as α and β, are in close agreement with those of the CO emission peaks.

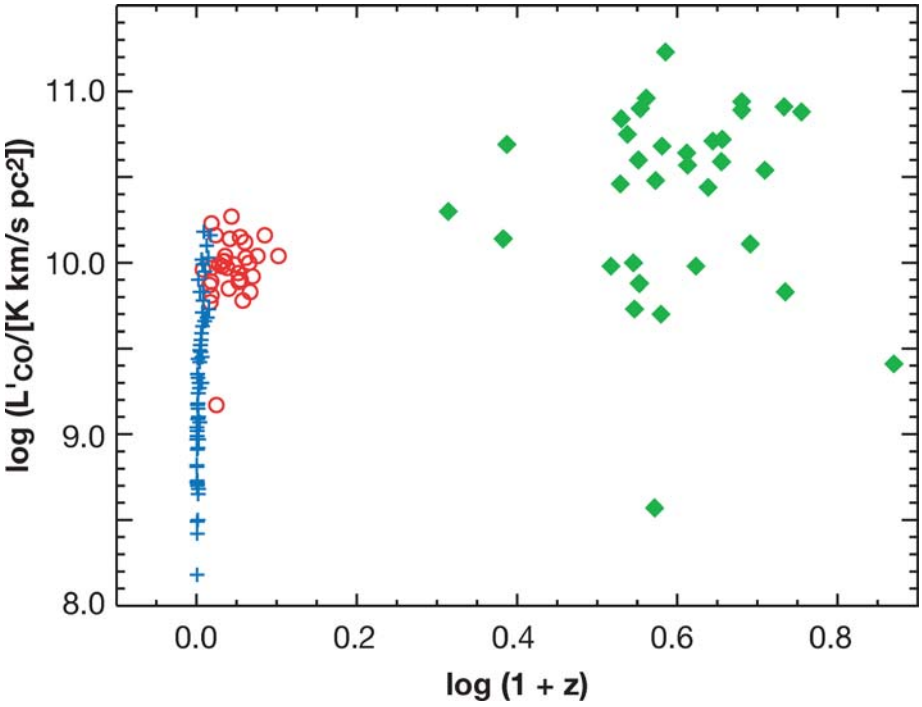

Figure 6 CO luminosity: log $L'_{\rm CO}$ versus log$(1 + z)$ for local galaxies with $L_{\rm FIR} < 10^{11.8}$ (*blue crosses*), ULIRGs (*red circles*), and EMGs (*green diamonds*). Although the EMGs are a flux-limited sample, the large scatter among the EMGs shows that they are much more diverse in CO luminosity and three times stronger in the mean compared with ULIRGs. The mean for ULIRGs and EMGs is 1×10^{10} and 3×10^{10} K km s^{-1} pc^2, respectively. All EMG luminosities with known lensing are corrected for magnification.

It is well known (Sanders et al. 1988, Sanders & Mirabel 1996, Solomon & Sage 1988) that the star formation efficiency of ULIRGS, which are mergers and closely interacting galaxies, is higher than that of normal spiral galaxies, and there is a well-established trend whereby star formation efficiency increases with increasing FIR luminosity. Figure 8, which shows log$(L_{\rm FIR})$ as a function of log$(L'_{\rm CO})$ for normal spirals, LIRGs, ULIRGs, and EMGs, extends the trend above 10^{13} $L_\odot$. The slope is 1.7, similar to that found without EMGs (Gao & Solomon 2004). This demonstrates that, given their high FIR luminosity, EMGs have the high star formation efficiency expected by extrapolation from low-redshift galaxies. Figure 8 also shows that EMGs with the same CO luminosity or molecular mass as ULIRGs also have the same (or slightly higher) FIR luminosity and star formation efficiency. They do not look like scaled-up versions of normal spirals with a larger molecular mass. The high star formation efficiency of luminous IR galaxies is due to a very high fraction of dense molecular gas as traced by HCN emission (Solomon,

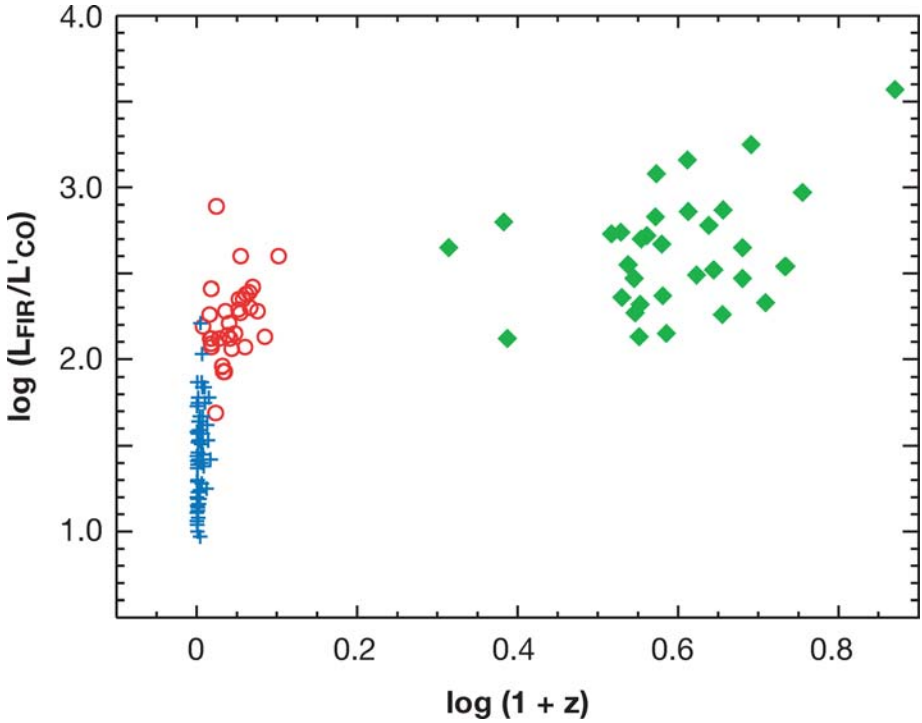

Figure 7 Star formation efficiency: $\log(L_{\rm FIR}/L'_{\rm CO})$ versus $\log(1+z)$ an indicator of star formation efficiency, for normal spirals including luminous but not ultraluminous galaxies (*blue crosses*), ULIRGs (*red circles*), and EMGs (*green diamonds*). ULIRGs and EMGs both have much higher star formation efficiency (SFE) than lower luminosity galaxies. EMGs have only a factor of 2 higher SFE on average than the EMGs, but there is substantial overlap even though the average FIR luminosity and star formation rate is 10 times higher for EMGs than ULIRGs.

Downes & Radford 1992c) (and other molecules), rather than the total molecular gas mass traced by CO emission. In this sense, CO luminosity is not a linear tracer of the star formation rate.

3.2. Star Formation and Gas Depletion Lifetime

The high star formation efficiency of EMGs also implies a short star formation lifetime. Taking the star formation rate to be given by $1.5\times10^{-10}L_{\rm FIR}$ ($M_\odot$ year^{-1}), see for example Kennicutt (1998), and using the above star formation efficiency $L_{\rm FIR}/L'_{\rm CO} = 350$ and $\alpha = 0.8$, the average star formation rate per solar mass of molecular gas $\approx 6\times10^{-8}$ year^{-1}. (This assumes that all FIR luminosity is due to star formation.) The inverse is the average star formation lifetime or average gas

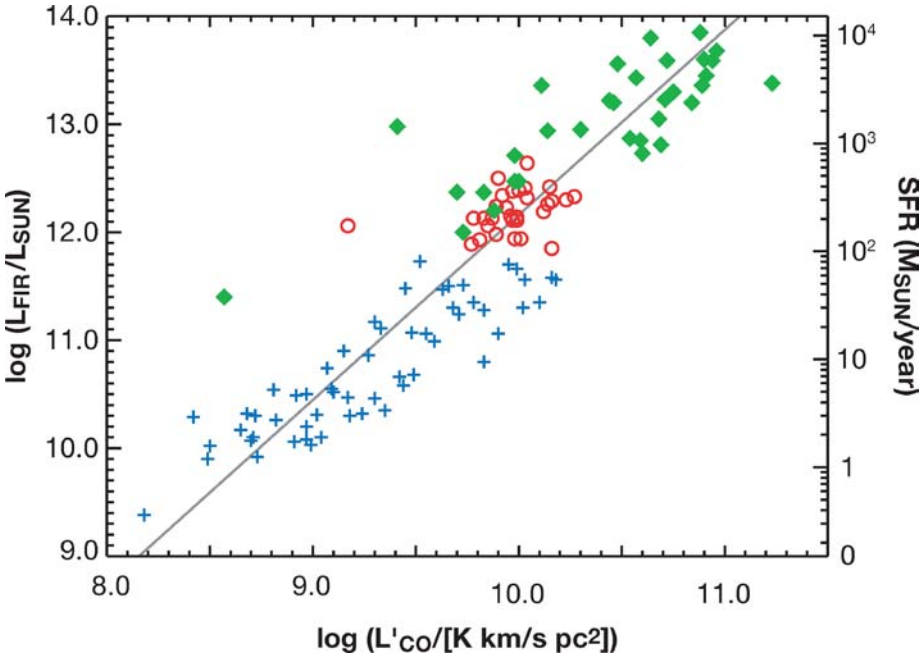

Figure 8 CO as a tracer of star formation rate: log $L_{\rm FIR}$ and star formation rate versus log $L'_{\rm CO}$ for normal spirals (*blue crosses*), ULIRGs (*red circles*), and EMGs (*green diamonds*). The *solid line* (a fit to all the points) has a steep slope, $\log L_{\rm FIR} = 1.7 \log L'_{\rm CO} - 5.0$, showing that total molecular mass indicated by CO luminosity is not a linear tracer of the star formation rate, indicated by FIR luminosity, when ULIRGs and EMGs are included. Excluding ULIRGS and EMGs the slope is 1.1. Unlike CO, HCN luminosity is a linear tracer of FIR luminosity and the star formation rate (see Section 3.2.1).

depletion time $\tau_{\rm SF} = 16$ My. Starbursts in EMGs are thus a brief but critical phase in galaxy formation and evolution.

Figure 9 shows the star formation lifetime of normal spirals, ULIRGs, and EMGs as a function of FIR luminosity. Because the CO to H_2, mass conversion factor is larger for normal spirals than for ULIRGs, α is treated as a parameter and the lifetime is normalized to $\alpha = 1.0$. For normal spirals $\alpha = 4.6$ and the gas lifetime will be larger than indicated. For ULIRGs and, presumably, EMGs the lifetime is close to that indicated. Normal spirals with dust-enshrouded star formation have gas depletion times in excess of 10^9 years, whereas ULIRGs and EMGS have lifetimes in the range of 10^7 to 10^8 years. For EMGs the lowest level CO line observed has been used to determine the molecular gas mass; to the extent that the CO(1–0) line luminosity is higher than the (3–2) or (4–3) line the gas mass and lifetime will be proportionally larger for some EMGs without CO(1–0) measurements. The few available (1–0) measurements indicate that this will be a

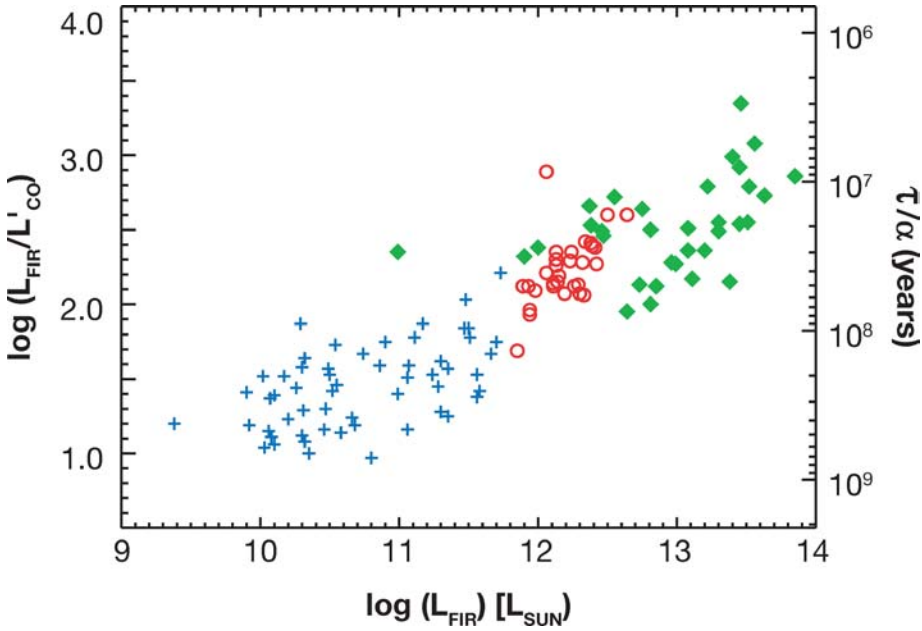

Figure 9 Star formation lifetime: star formation lifetime τ due to gas depletion versus log $L_{\rm FIR}$ for normal spirals (*blue crosses*), ULIRGs (*red circles*), and EMGs (*green diamonds*). α is the CO line luminosity to H_2 mass conversion factor (see Section 2.2), which is about 0.8 for ULIRGS, probably 0.8 for EMGs and 4.6 for normal spirals. The EMG star formation lifetime is between 10^7 and 10^8 years (see the text). The star formation rate can be taken as $1.5 \times 10^{-10}\ L_{\rm FIR}\ [M_\odot\ {\rm year}^{-1}]$.

small effect (less than a factor of 2) for most sources. (This short lifetime also sets limits on the dimensions of the starburst because the dynamical time must be less than the starburst lifetime.)

3.3. HCN, CI, and CII Emission

3.3.1. HYDROGEN CYANIDE: DENSE MOLECULAR GAS HCN emission traces dense gas, $n(H_2) > 3 \times 10^4\ {\rm cm}^{-3}$ generally associated with the star-forming cores of GMCs, whereas CO, with its low dipole moment, can have emission excited by gas at the much lower densities found in GMC envelopes. HCN line luminosity is a much more specific tracer of star formation than is CO luminosity, although CO is a better overall tracer of total molecular mass. In normal spirals and luminous infrared galaxies (LIRGs and ULIRGs), the correlation between FIR luminosity and HCN line luminosity is much tighter than that of FIR with CO line luminosity (Gao & Solomon 2004; Solomon, Downes & Radford 1992c). The star formation rate deduced from the IR luminosity scales linearly with the amount of dense

molecular gas traced by HCN emission over more than three orders of magnitude in IR luminosity from $10^{9.3}$ to $10^{12.3}$ $L_\odot$. This is not the case for CO emission, which shows much higher star formation efficiencies indicated by $L_{\rm FIR}/L'_{\rm CO}$, for luminous IR galaxies than for normal galaxies. In particular, ULIRGs have a star formation efficiency or rate of star formation per solar mass of molecular gas that is, on average, five times higher than that of normal galaxies. Luminous IR galaxies have a huge HCN line luminosity, large mass of dense gas, and a high ratio of dense gas to total molecular gas indicated by $L'_{\rm HCN}/L'_{\rm CO}$; for ULIRGs this luminosity ratio is typically one fourth to one eighth, whereas for normal spirals it is in the range 1/25 to 1/40. The ULIRG Mrk 231 often regarded primarily as an AGN has a ratio $L'_{\rm HCN}/L'_{\rm CO} = 1/4$ and an HCN luminosity much larger than the CO luminosity of the Milky Way. This finding led Solomon, Downes & Radford (1992c) to conclude that even this galaxy with a definite AGN had most of its bolometric luminosity supplied by a starburst. This has recently been confirmed by near-IR spectroscopy of the Mrk 231 starburst disk (Davies, Tacconi & Genzel 2004). All galaxies in the local Universe with global ratios $L'_{\rm HCN}/L'_{\rm CO} \geq 1/14$ are luminous or ultraluminous IR starburst galaxies (Gao & Solomon 2004).

HCN observations of EMGs provide an important test of the star formation model. The fact that the ratio of IR luminosity to HCN luminosity in ULIRGs is the same as in lower luminosity normal spiral galaxies shows that ULIRGs, like the lower luminosity galaxies, are primarily powered by star formation and that the HCN line luminosity is a good measure of the mass of actively star-forming cloud cores (Gao & Solomon 2004; Solomon, Downes & Radford 1992b). The star formation that is responsible for the FIR emission has a rate that is linearly proportional to the HCN luminosity tracing the mass of dense molecular gas but not to the total molecular gas as traced by CO. HCN observations can address the question of whether EMGs have a sufficient mass of dense molecular gas to account for the huge IR luminosity by star formation.

HCN(1–0) emission has been detected from three EMGs: the Cloverleaf (Solomon et al. 2003), F10214 (Vanden Bout, Solomon & Maddalena 2004), and VCV J1409 (Carilli et al. 2004). In all three cases, the HCN(1–0) line luminosity is larger by a factor of 100 (or more) than that of normal spiral galaxies and a few times that of the ULIRG Arp 220, indicating the presence of a large mass of dense molecular gas. Based on the FIR luminosity (not the mid-IR from very hot dust), the rations of $L_{\rm FIR}/L'_{\rm HCN} = 1700$ and 2700 for the Cloverleaf and F10214, respectively, are only slightly higher than that of Arp 220 or the average for local ULIRGs. The dense gas fraction indicators $L'_{\rm HCN}/L'_{\rm CO} = 1/14$ and 1/6, respectively, denote starbursts in both systems. Detailed discussions of the HCN in these two objects are given in Section 2.4. The third detection VCV J1409 shows not only the highest HCN luminosity (assuming no magnification by a gravitational lens), but also a somewhat higher $L_{\rm FIR}/L'_{\rm HCN} = 4000$, approximately a factor of 3 above the average for local IR starbursts. Using a dense gas conversion factor for the HCN luminosity $\alpha_{\rm HCN} \approx 7\ M_\odot$ (K km s^{-1} pc^2)$^{-1}$ (Gao & Solomon 2004) leads to a dense gas mass of 1, 4, and $5 \times 10^{10}\ M_\odot$ for F10214, the Cloverleaf, and VCV J1409, respectively, where the mass of dense gas in VCV J1409 assumes

no magnification by a gravitational lens. Assuming that all the FIR luminosity is from star formation leads to lifetimes for the dense gas of approximately 1–2 $\times$ 10^7 years.

There are four other EMGs with upper limits for HCN (Carilli et al. 2004, Izaak et al. 2002); all seven high-z sources including the upper limits are within the range expected from an extension of the low-z galaxy FIR-HCN linear correlation if star formation is responsible for most of the FIR luminosity (Carilli et al. 2004).

3.3.2. ATOMIC CARBON Observations of the forbidden fine-structure lines of neutral atomic carbon in the Milky Way and nearby galaxies (Ojha et al. 2001, Gerin & Phillips 2000, and references therein) have revealed a close association with CO emission. Because the critical density for excitation of both the [CI] ($^3P_1 \rightarrow {}^3P_0$) transition at 492.160 GHz and the ($^3P_2 \rightarrow {}^3P_1$) transition at 809.342 GHz is roughly that of CO(1–0), these observations suggest that the CO and [CI] emissions originate in the same volume. This fact presents the opportunity to examine the emission region independently of CO, in a pair of optically thin lines that can be used to infer CI excitation, physical conditions, and mass. In EMGs, the large redshift eliminates the burden of working at the [CI] rest frequencies, which fall in regions where Earth's atmosphere makes observations difficult. Papadopoulos, Thi & Viti (2004) have discussed the utility of the [CI] lines for the study of EMGs.

The [CI] ($^3P_2 \rightarrow {}^3P_0$) emission has been observed in five ULIRGs (Gerin & Phillips 2000; Papadopoulos & Greve 2004), where inferred masses of molecular gas from the [CI] observations assuming a relative abundance of CI to H_2, $X(\mathrm{CI}) = 3 \times 10^{-5}$, the value inferred for M82 (Weiß et al. 2003), agree well with those from CO assuming $\alpha = 0.8$, the value usually adopted for ULIRGs. This further supports a common emission region hypothesis.

If the CI levels are thermally populated, then the excitation temperature can be calculated from $T_{\mathrm{ex}} = 38.8\ \mathrm{K}/\ln(2.11/R([\mathrm{CI}]))$, where $R([\mathrm{CI}])$ is the ratio of (2–1) to (1–0) integrated line intensities (Stutzki et al. 1997). CI masses can be calculated from

$$M(\mathrm{CI}) = 0.911 \times 10^{-4} Q(T_{\mathrm{ex}})\, \mathrm{e}^{62.5/T_{\mathrm{ex}}} L'[\mathrm{CI}](^3P_2 \rightarrow {}^3P_1)[M_\odot],$$

$$M(\mathrm{CI}) = 1.902 \times 10^{-4} Q(T_{\mathrm{ex}})\, \mathrm{e}^{23.6/T_{\mathrm{ex}}} L'[\mathrm{CI}](^3P_1 \rightarrow {}^3P_0)[M_\odot],$$

where $Q(T_{\mathrm{ex}}) = 1 + 3\,\mathrm{e}^{T_1/T_{\mathrm{ex}}} + 5\mathrm{e}^{T_2/T_{\mathrm{ex}}}$ is the CI partition function (Weiß et al. 2005).

Four EMGs have been observed in [CI] emission: the Cloverleaf, F10214, SMM J14011, and PSS J2322 (Barvainis et al. 1997; Pety et al. 2004; Weiß et al. 2003, 2005). Only the Cloverleaf has been observed in both [CI] lines, with an inferred excitation temperature of 30 K, somewhat colder than the fit to the SED dust component of 50 K (Weiß et al. 2003). Assuming the same T_{ex} for the Cloverleaf and F10214, and using CO data to infer the mass of H_2, Weiß et al. (2005) found carbon abundances for all three of $X[\mathrm{CI}]/X[\mathrm{H_2}] \sim 5 \times 10^{-5}$, assuming $\alpha = 0.8$, the ULIRG value, and ignoring differential magnification of [CI] and CO. The carbon abundance in PSS J2322 is 3×10^{-5} (Pety et al. 2004), close to the value

for the other three detections. This is an indication of substantial enrichment in heavy elements as early as $z \sim 2.5$. Within the uncertainties, there are no strong differences in the properties inferred from [CI] observations between the three QSOs and the SMG in the sample of four.

Theoretical models predict that CII emission in the $(^2P_{3/2} \rightarrow {}^2P_{1/2})$ fine-structure line at 1900.54 GHz is an important coolant for the photo-dissociation regions of molecular clouds, more important than the emission lines of either CO, [CI], or other atomic fine-structure lines. CII emission has been observed in galactic molecular clouds, normal galaxies, and ULIRGs. The bulk of the extragalactic observations were made with the Infrared Space Observatory (ISO) and show that ULIRGs are weaker in CII than might be expected from a simple extrapolation from the Milky Way (for a review see Malhotra 2000). Only upper limits have been obtained for [CII] emission in EMGs (DJ Benford et al., mansucript submitted; van der Werf 1999). A search for CII emission in SDSS J1148 (Bolatto, Francesco & Willott 2004) yielded an upper limit that suggests that the weakness of CII emission in ULIRGs persists to redshifts as high as $z \sim 6$. However, even at the current upper limits, CII remains the dominant coolant, roughly twice as important as CO and CI combined (Pety et al. 2004). This is an area where the sensitivity of ALMA is required for significant progress.

3.4. Masses, Sizes, and Evolutionary Destiny

Size measurements of CO emission from EMGs are constrained by the limited resolution and sensitivity of existing telescope arrays. In strongly lensed systems this limitation can be overcome, and effective angular resolution of the source can be 10 or more times greater than the instrumental resolution of the magnified image. Derived source diameters then depend on the accuracy of available lensing models. For most EMGs, the measured CO sizes provide only upper limits. There are a few EMGs, including two radio galaxies without lensing and two SMGs, where CO measurements indicate extended or complex CO morphology. There is also indirect evidence of extended, large molecular gas disks from measurement of extended nonthermal radio continuum (Chapman et al. 2004) and, by implication, extended FIR and CO emissions based on the radio-FIR correlation (Carilli, Menten & Yun 1999). We concentrate here on direct CO measurements of the size and/or separation between the components of the molecular gas. The CO kinematics also make it possible to estimate a dynamical mass that is independent of the gas mass determined from the CO line luminosity.

The size and mass of the molecular gas disks are important factors in determining the evolutionary state of EMGs. Local IR galaxies and, in particular, ULIRGs share many of the properties of this high-redshift sample. They have luminosities greater than $10^{12}\ L_\odot$ (Sanders & Mirabel 1996), and in a large sample all but one are CO luminous (Solomon et al. 1997), with an average gas mass of $7 \times 10^9\ M_\odot$ (using the conversion factor adopted in Section 2.2). The molecular gas is in centrally concentrated rotating disks with characteristic diameters of 0.7–2.5 kpc

(Downes & Solomon 1998), although molecular emission extends out about twice this far. ULIRGs result from the merger of two gas-rich spiral galaxies (Sanders & Mirabel 1996) in which the gas is driven toward the center. The large gas mass and presence of ample dense molecular gas (Gao & Solomon 2004) lead to models where most of the FIR luminosity is derived from a starburst, but some ULIRGs are clearly composite AGN-starburst sources. Although the properties of ULIRGS and EMGs overlap, many EMGs are more extreme objects than are ULIRGs with higher IR and CO luminosities, implying higher star formation rates and higher molecular gas mass. This leads to suggestions that the submillimeter population or some portion of it represents the formation of giant (>L*) elliptical galaxies (Genzel et al. 2003, Greve et al. 2005, Neri et al. 2003, Papadopoulos et al. 2000), clearly not what is happening in ULIRGs.

3.4.1. SUMMARY OF MOLECULAR GAS MASS (H_2 + He) Figure 10 shows the gas mass (H_2 + He) derived from the CO luminosity for the ULIRGs and EMGs

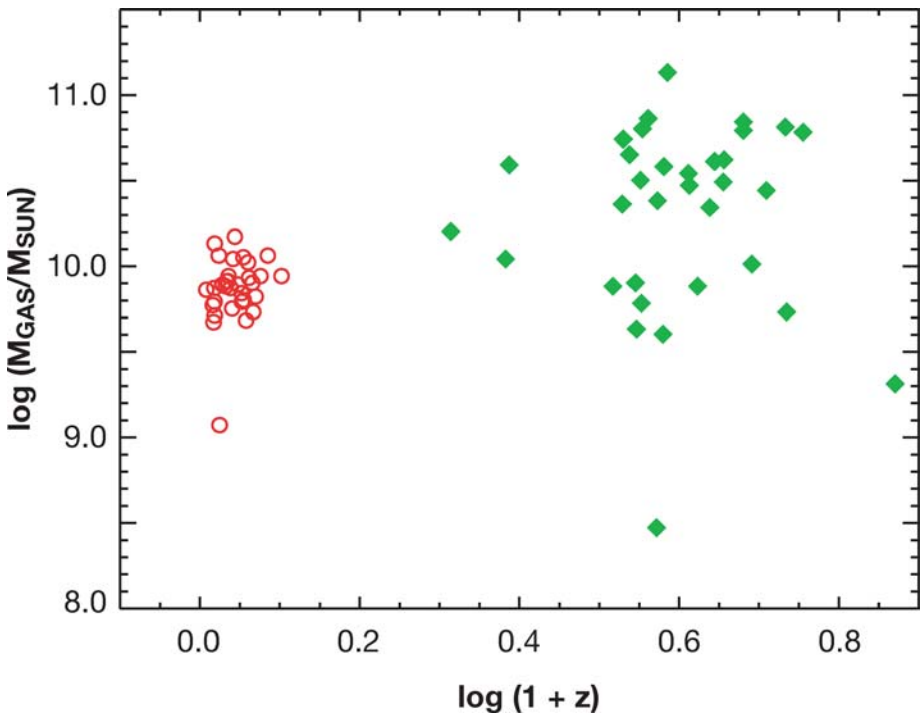

Figure 10 Molecular gas mass in ULIRGs and EMGs: log $M_{\rm gas}$ versus log(1 + z) for ULIRGs (*red circles*) and EMGs (*green diamonds*). $M_{\rm gas}$ includes H_2 and He. The EMGs are more massive on average than the ULIRGs, although there is considerable scatter among individual EMGs and substantial overlap with ULIRGs (see the text).

as a function of redshift. In cases where the magnification has been estimated the figure shows the intrinsic mass. Otherwise a magnification of one is assumed. There are 11 EMGs with a gas mass essentially the same as that of local ULIRGs. As discussed in the previous section, most of these (8 of 11) have the same or slightly higher FIR luminosities as that of ULIRGs. One galaxy has a gas mass 10 times less than a typical ULIRG, similar to an ordinary spiral. This object (cB58) is a Lyman Break galaxy with a very large magnification and is clearly not part of the EMG population because it is not a molecular gas-rich galaxy. There are 21 EMGs with a molecular gas mass significantly higher than that found in ULIRGs and higher than that of any galaxy in the local Universe. They range in gas mass from about 2.5 to $10 \times 10^{10}\ M_{\odot}$. They include SMGs, radio galaxies, and molecular disks associated with a few quasars. Some of these systems have multiple components and may represent interacting or merging galaxies. A few may have lensing not yet detected or with a magnification not properly estimated.

3.4.2. SIZE MEASUREMENTS AND DYNAMICAL MASS Table 2 summarizes the observed sizes of the CO emission regions excluding galaxies with upper limits. The full range of source diameters is from 0.8 to 16 kpc, with all but two of the diameters falling between 1 and 5 kpc. The highly magnified CO emission associated with some quasars in Table 2 has sizes for the molecular rings or disks comparable to nearby ULIRGs. The dynamical masses listed in Table 2 have been calculated from $M_{\rm dyn} \sin^2 i = 233.5\ R\Delta V^2$, where R is either the radius of the molecular disk or half the separation between components in a merger model, measured in parsec, and ΔV is the FWHM of the CO line profile or half the separation in velocity of the component CO lines in a merger model, measured in kilometers per second. The unknown geometry of these systems precludes more accurate estimates. Footnotes are given for those cases where this calculation yields a result differing substantially from that in the reference cited. The gas masses for this subset with measured sizes are the same as those in Table 1 and Figure 10.

The largest source is the SMG J02399 with a diameter of 16 kpc (Genzel et al. 2003) after allowing for a magnification of 2.5 due to the intervening cluster lens. The size is obtained from the CO data by fitting a model of a rotating disk with a velocity of 420 km s^{-1}, a flat rotation curve, and a large turbulent velocity. This leads to a molecular ring with a maximum gas density at $R = 3.2$ kpc and a width of 1–1.5 kpc. The 6–8 kpc outer radius for the gas also matches the extent of the submillimeter dust continuum. The ring is required to fit the double-peaked line profile. This large disk size is the total extent rather than the half power diameter, which is only $\sim$1 kpc larger than the peak of the ring corresponding to a half power diameter of 8 kpc. Although Genzel et al. (2003) stress the rotating molecular starburst ring model with an AGN at the center of the ring, an alternative configuration with two galaxies orbiting each other with the AGN in either the red- or blueshifted CO source is possible. Indeed, the double-horned line profile with a steep drop in the middle and the position velocity diagram could easily be due to

TABLE 2 Dynamical masses and size

EMG	M_{gas}[a] ($10^{10}\,M_\odot$)	$M_{dyn}\sin^2 i$[b] ($=R(\Delta V)^2G^{-1}$) ($10^{10}\,M_\odot$)	Source size: Inferred disk diameter (kpc)	Source size: Observed component separation (kpc)	Lens magnification used
SMM J02396	1.7	3.6	—	9.1	2.5[c]
F10214	0.5	0.5	0.8	—	17[d]
SMM J16359	0.5	0.7	3.0	—	45[e]
Cloverleaf	1.9	2.5	1.5	—	11[f]
SMM J14011	0.3–1.5	0.3–1.5	0.7–7.0	—	2.5–25[g]
SMM J02399	4.0	32	16	—	2.5[h]
4C60.07	$4+7=11$	10–43	—	7–30[i]	1
4C41.17	$3+3=6$	6[j]	—	13	1
APM 08279	1.5	6.4[k]	2.0	—	7[j]
PSS J2322	3.9	3.0	4.0	—	2.5[k]
BRI 1335	$2.6+3.8=6.4$	18	—	8.7	1
BR 1202S	$4.2+3.7=7.9$	0.8	—	1.9	1
SDSS J1148[l]	1.5	4.4	4.6	—	1
SDSS J1148[m]	$0.5+0.5=1.0$	1.5	—	1.7	1
ULIRGs (FWHM)[n]		0.7–2.0	0.8–2.4	—	1
ULIRGs (total)[p]	0.5–1.5	2–7	2.4–6.8	—	1

[a]From Table 1, where $M_{gas} = M(H_2)$ corrected to include He; [b]R = disk radius; ΔV = FWHM of line profile or half the velocity separation of components; [c]Kneib et al. (1993); [d]D Downes & PM Solomon, manuscript in preparation; [e]Kneib et al. 2004b; [f]Venturini & Solomon (2003); [g]Downes & Solomon (2003); [h]Genzel et al. (2004); [i]Range reflects change in component separation with image tapering; [j]Lewis et al. (2002), authors used HWHM velocity, yielding $M_{dyn} = 1.5 \times 10^{10}\,M_\odot$ after adjusting for cosmology; [k]Carilli et al. (2003); [l]Low resolution (1.5″) image; [m]High resolution (0.15″) image; [n]For radius at half maximum of gas density; [p]For radius of full extent of gas.

two separate galaxies, each with a much smaller unresolved CO disk or ring. Thus, it is not clear if the quoted diameter is a separation between two unresolved disks or a disk size. The dynamical mass for a merger model is $M_{\rm dyn} \sin^2 i \sim 3 \times 10^{11}\ M_\odot$.

The other SMG with a measured CO size is J14011. Ivison et al. (2001) found a CO(3–2) size of 6.6″ corresponding to 56 kpc in the image plane and 22 kpc in the source after accounting for magnification by a factor of 2.5 due to the intervening cluster Abell 1835. If real, this would have been the largest high-redshift galaxy found at any wavelength. Downes & Solomon (2003) using the IRAM interferometer mapped both the (3–2) and (7–6) lines with high sensitivity and resolution. They measured the peak flux to an accuracy of 14σ and found an image size of $2'' \times \leq 0.5''$. For magnification as small as 2.5, the intrinsic source diameter is reduced to less than 7 kpc. Downes & Solomon (2003) also suggested a lensing model with an intervening galaxy in addition to the cluster lens. The total magnification was $25 f_{\rm v}$, where $f_{\rm v}$ is the velocity filling factor of the CO emission. This model, with increased magnification by an intervening galaxy, has been questioned (Genzel et al. 2003, Tecza et al. 2004), but Tecza et al. (2004) increased the expected cluster magnification to 5. In Table 2 we treat the magnification of J14011 as uncertain, with a maximum of 25 and a minimum of 5. This reduces the source diameter to the range of 0.7–3.5 kpc. The molecular mass is in the range of 0.4–1.7 $\times\ 10^{10}\ M_\odot$. The observed CO spectral line is narrow with an FWHM of 190 km s^{-1} (Downes & Solomon 2003), indicating a moderate dynamical mass of about $3 \times 10^{10}\ M_\odot$ for an assumed inclination of 45° and the larger diameter of 3.5 kpc. Unless the disk is completely face on and/or has the magnification much lower than 5, the dynamical mass is similar to that of ULIRGs such as Mrk 231, Arp 220, VII ZW31, or IR23365 + 36 (Downes & Solomon 1998).

As part of a large survey of CO emission from SMGs, Greve et al. (2005) summarized the measured linewidth and CO luminosity of 11 SMGs. They found a large median linewidth of 780 ± 330 km s^{-1} (FWHM), 2.5 times larger than the median width for local Universe ULIRGs, with several examples of double-peaked profiles. The largest linewidth for an ULIRG in a sample of 37 galaxies is 480 km s^{-1}. The SMG sample also has a high median CO line luminosity (3.6×10^{10} K km s^{-1} pc^2) with a median molecular mass of $3 \times 10^{10}\ M_\odot$, four times higher than the ULIRG mean (Solomon et al. 1997). Although Greve et al. (2005) concluded that this is sufficient gas mass to form the stars of a giant elliptical galaxy, it seems small unless most of the mass is already in stars and the SMGs represent a late stage of galaxy formation. The large linewidths indicate a large but very uncertain dynamical mass, owing to the absence of size measurements and unknown geometry. Assuming a separation (diameter) of 3.7 kpc, Greve et al. (2005) gave a median dynamical mass $M_{\rm dyn} \sin^2 i = 1.2 \times 10^{11}\ M_\odot$.

There are some IR luminous interacting galaxies in the local Universe with very large linewidths similar to the EMGs; one example is the LIRG Arp 118 (NGC1144)—an unusual ring galaxy with a total CO linewidth of 1100 km s^{-1}

and an FWHM of $\sim$750 km s^{-1}. Whereas the linewidths of the SMG population are similar, the SMG population is more than one order of magnitude higher in luminosity.

The most impressive measurement in Table 2 is the size and structure of the CO(3–2) emission from the $z = 6.4$ quasar J1148 + 52. Walter et al. (2004) mapped the CO(3–2) line with a resolution of 0.3″ and 0.15″; the latter is equivalent to $\sim$1 kpc. The results show a disk with a maximum diameter of 4.8 kpc and an FWHM of 3.5 kpc. The entire disk is two to three times as large as a typical ULIRG. The core region shows two distinct sources separated by 1.7 kpc with a size of roughly 0.5 kpc that accounts for half of the total emission. Each of these regions is similar to a nearby ULIRG in terms of mass, intrinsic brightness temperature, and size (Walter et al. 2004). A detailed comparison with ULIRGs suggests that each of these components may resemble the core of the molecular region in an ULIRG rather than the whole disk.

Some of the high-z radio galaxies show kinematic structure indicating the presence of two merging galaxies. In 4C41.17 (De Breuck et al. 2004) the two CO components are separated by 1.8″ or 13 kpc with a velocity difference of 500 km s^{-1}. Each component has a molecular mass of approximately $3 \times 10^{10}\ M_{\odot}$. This system appears to be a major merger in progress between two gas-rich galaxies rather than one extended very massive disk. Each component remains unresolved. The dynamical mass of the system is $M_{\rm dyn} \sin^2 i = 6 \times 10^{11}\ M_{\odot}$.

4C60.07 also shows possible evidence of an ongoing merger between two galaxies, although the angular separation between the components is not well determined. Papadopoulos et al. (2000) imaged the CO(4–3) line and found an extent or separation of 7″ or 51 kpc, but the resolution of the measurements was only 9″ × 5.5″. Higher resolution measurements in the CO(1–0) line (Greve, Ivison & Papadopoulos 2004) show a separation of 4″ or $\sim$28 kpc in the images tapered to 60 kλ; the higher resolution images tapered to 200 kλ show a smaller angular separation of only $\sim$1″. Using the larger separation they calculate a total dynamical mass between 0.2 and $0.8 \times 10^{12}\ M_{\odot}$ comparable to the mass of a giant elliptical galaxy.

In Table 2 we list two size ranges for ULIRG molecular disks in the local universe, including the half power diameter and the total diameter for CO emission. The measured diameters of EMGs fit within the range measured for ULIRGs with one noticeable exception. The total gas mass of EMGs covers a wide range. About half of the EMGs have a total gas mass above that found for any local ULIRG and thus represent the largest reservoirs of star forming molecular gas in the universe.

3.4.3. ARE EMGs MASSIVE GALAXIES IN FORMATION? A critical question is whether the EMGs or some fraction of the EMGs represent the formation of massive galaxies in the early Universe. The star formation rates derived from the FIR luminosity range from approximately 300 to 5000 $M_{\odot}$ year^{-1} (see Figure 8). At the lower

end, these star formation rates are similar to local ULIRGs and represent starbursts in centrally concentrated disks sometimes but not always associated with AGNs. These events may form a central bulge but not a giant elliptical galaxy. At the higher end, it would take 10^8 years to produce a stellar mass of 3–5 $\times$ 10^{11} $M_\odot$ typical of the stellar mass of a giant elliptical galaxy. This is a reasonable timescale. However, the available molecular gas supply, approximately 3–6 $\times 10^{10}$ $M_\odot$, falls short by a factor of 5–10. The gas lifetime is too short. The remaining 80–90% of the mass would already have to be in the stellar component of the EMGs or added later by subsequent mergers in order to account for the formation of a giant elliptical galaxy. Accurate measurements of the dynamical mass and size scale of EMGs are needed to provide convincing evidence for EMG masses similar to modern elliptical galaxies. Table 2 shows five EMGs with the approximate dynamical mass in the right range, but the size measurements are only marginally significant in most cases. The large linewidths of the SMG population (Greve et al. 2005) are a good indication that the total mass of some of these early galaxies is large, but most of these have unknown morphology and do not have size measurements. CO images with substantially higher resolution and sensitivity are required.

The EMG population clearly represents a major stage in galaxy formation. The high star formation rates, high total molecular mass, and, in some cases, high mass of dense molecular gas all point to huge starbursts, much greater than observed in individual optical-UV starbursts.

3.4.4. COMPARISON WITH LYMAN BREAK GALAXIES The distribution of star formation rates from LBGs obtained directly from the UV flux shows a peak at about 20 $M_\odot$ year^{-1}, falling off rapidly for higher star formation rates (Giavalisco 2002). Correction for extinction involving dust scattering models and stellar population synthesis shifts the peak to about 100 $M_\odot$ year^{-1} with a broad distribution and a tail extending up to about 700 $M_\odot$ year^{-1}. In the most extreme cases the UV radiation captures much less than 10% of the total luminosity with the rest shifted into the IR. Tests of this extinction correction technique show that it fails completely for local ULIRGs (for example, Giavalisco 2002) and would also fail for EMGs. The range of star formation rates for EMGs begins at the higher end of the extinction-corrected UV values for LBGs and extends upward by an order of magnitude. Giavalisco (2002) suggests that the star formation observed in LBGs could lead after 1 Gyr to an L* galaxy. But there is no evidence for the presence of sufficient interstellar gas in LBGs to build up an L* galaxy. The one LBG found with CO emission, MS1512-cB58 (see Table 2), contains only a few $\times 10^8$ $M_\odot$ of molecular gas, 30 times less than the mean of the EMG sample (this EMG appears as a low outlier in Figure 6), and more than two orders of magnitude below the mass of an L* galaxy.

The total contribution to early Universe star formation from SMGs compared with LBGs depends on an understanding of the origin of the FIR background, a topic addressed elsewhere (Puget & Lagache 2005).

4. OBSERVATIONAL PROSPECTS

Observations of the molecular gas discussed here are critical for understanding early Universe galaxy formation. The morphology, kinematics, and gas density estimates provided by better measurements of CO and other molecular lines will lead to a detailed understanding of the processes and mechanisms involved in assembling galaxies and forming stars in the early Universe.

The present suite of telescopes available for the detection of EMGs has produced a sample of 36, which is expected to grow, particularly for SMGs, within the limits of the observing time allocated for high-z CO emission searches. A doubling of the sample is not unreasonable to expect in the next 5 years. But this falls far short of the sample sizes needed for true statistical studies of EMG properties. The current sample is especially deficient at redshifts $z > 3$, where the potential of the EMGs for the study of galaxy formation is most important. There is only one EMG that probes the era of re-ionization.

Besides their limitations for the detection of more EMGs, the ability of the present telescopes to study these objects in detail is severely limited in sensitivity and angular resolution. Only the strongest sources, observed at high frequencies, possibly through gravitational lenses, and with long integration times, offer clues regarding the structure of EMGs. To understand EMGs, images that resolve and map the molecular line emitting region are critical.

ALMA is the only observing facility planned for operation within the next decade that combines the sensitivity, angular resolution, flexibility of observing modes, and site conditions required for such imaging. ALMA will be the premier telescope for the study of EMGs. Its 64 12-m-diameter antennas provide the collecting area needed for high sensitivity. The ability to reconfigure the array allows one to select angular resolution for any observing frequency. The angular resolution at a frequency of 350 GHz is $1''$ in the compact configuration, as high as $0.014''$ using baselines up to the maximum of 14 km, and scaling inversely with frequency. The correlator can process up to 16 GHz of bandwidth from each antenna, in four separately tunable 2-GHz-wide signals in each of the two polarizations. The receiver noise will be three times the quantum limit ($T_{rx} \approx 3h\nu/k$) for all but the highest frequency receiver bands. A compact array of 12 7-m-diameter antennas, plus four 12-m-diameter antennas for calibration purposes, bolsters sensitivity on spatial frequencies between that of a single 12-m antenna and the shortest baseline (15 m) in the large array. The site is comparable in quality to the South Pole for millimeter/submillimeter observing and superbly located for studying the southern sky and much of the northern sky. For further information on ALMA, the reader is referred to http://www.alma.nrao.edu/ and http://eso.org/projects/alma/.

Guilloteau (2001) and Blain (2001) have reviewed ALMA's ability to observe high-z spectral line and continuum emissions, respectively. As an illustration of ALMA's power for detailed studies of EMGs, consider the SMG J23099, where the CO source has been modeled (Genzel et al. 2003) as a rotating disk of diameter 16 kpc ($5''$). When used in a 6-km-maximum baseline configuration with an

8-h integration, ALMA will yield an image with velocity resolution of 100 km s^{-1} and root-mean-square noise of 0.4 mJy (5σ). This is 10% of the unresolved flux density of the source, enough to check the validity of the model. Because this observation can be done with only one of the tunable 2-GHz inputs to the correlator, simultaneous observations of, say, CS(7–6), HCN(4–3), and up to 29 other lines within the instantaneous bandpass of the receiver could be made. Although these lines may not be detected in a single 0.5″ beam, the *U–V* data, fully sampled to 6 km, could be smoothed to 1″ resolution, thereby yielding a 5σ sensitivity of 0.1 mJy.

For simple detection of EMGs in CO emission, the (6–5) transition, for example, at a redshift of $z = 2$ with a peak line intensity of 1 mJy $beam^{-1}$ (or any spectral line in the bandpass with this peak line strength) would be seen by ALMA at the 10σ level with velocity resolution of 50 km s^{-1} in a typical 4-h observing session. The continuum emission observed in this same session at 230 GHz would reach a 5σ sensitivity of 33 μJy $beam^{-1}$. The continuum emission from Arp 220 moved to a redshift of $z = 2$ could be detected at the 5σ level in less than 30 min of observing time. Because of the "negative K-correction," this statement is true for Arp 220 at any redshift up to $z \sim 20$.

Given the sensitivity of ALMA, with seven times the collecting area of the IRAM interferometer and a superior site, it is clear that the study of EMGs will be transformed from one of imaging CO emission to one of imaging emission from a variety of interstellar molecules. The importance of HCN, CI, and CII has been discussed above. Carbon monosulfide may be an even better tracer of dense star-forming gas than is HCN (Shirley et al. 2003), but its weaker lines remain beyond the reach of present telescopes. Formaldehyde (H_2CO) is another molecule that traces dense gas, potentially accessible to ALMA observers of EMGs. Finally, searches should be made with ALMA for the isotopomers of CO. The ALMA correlator can observe many lines simultaneously, making it very powerful for astrochemical studies.

The potential for ALMA to reveal the process of galaxy formation and evolution in the early Universe can be summarized by noting that observing CO emission in the $z = 6.4$ quasar SDSS J1148 tests limits of present instruments. ALMA will be able to observe CO in a galaxy at this redshift having the CO luminosity of a large, normal spiral such as M51 or NGC 891, making it possible to probe the era of re-ionization with a much larger population. Readers who wish to design their own ALMA observing programs can find a sensitivity calculator at http://www.eso.org/projects/alma/science/bin/sensitivity.html.

Other facilities will also play a significant role in the study of EMGs. An upgraded IRAM interferometer, Combined Array for Research in Millimeter-wave Astronomy (CARMA), the Submillimeter Array (SMA), and the Extended VLA (EVLA) will add increased sensitivity and/or bandwidth to present capability. For objects with redshift $z \geq 2$, CO emission from low-J levels falls in the centimeter wavelength observing bands of the EVLA. The EVLA will be particularly suitable for observing HCN in lower-J transitions. Receiver systems working to wavelengths as short as 0.7 cm combined with a powerful wide-band correlator will

make the EVLA a powerful telescope of choice for EMG observing in the Northern Hemisphere. Large single dishes such as the Green Bank Telescope (GBT) are also proving useful for EMG study, as the detection of HCN(1–0) emission in F10214 (Vandenbout, Solomon & Maddalena 2004) has demonstrated. The GBT will be primarily useful for measuring CO(1–0) luminosity, detecting new EMGs in that line, and doing continuum surveys with 3-mm wavelength bolometer cameras. Upon completion, the 50-m diameter Large Millimeter Telescope (LMT) will be the most powerful single-aperture telescope for the study of EMGs. Its very substantial collecting area will make it a premier telescope for blind surveys.

The next decade will see explosive growth in the number of known EMGs, the findings concerning their properties, and most important, the knowledge of their structure and evolution. The ability of ALMA to image the kinematics of the molecular star-forming gas in galaxies from the era of recombination to the present will be invaluable to our understanding of the evolution of galaxies and the Universe.

ACKNOWLEDGMENTS

We gratefully acknowledge the assistance of J.W. Barrett in the preparation of the figures. P.V.B. is grateful for the hospitality of the Institut d'Astrophysique, Paris, and the Department of Astronomy, University of Texas, Austin, during the writing of this review.

APPENDIX 1 Early (universe) molecular (line emission) galaxies

	CO coordinates				
EMG[a]	**R.A. (2000)**	**Decl. (2000)**	**Redshift z(CO)**	**Galaxy type**	**Lensed? (μ = mag.)**
SMM J02396[b]	02:39:56.59	−01:34:26.6[b]	1.062 ± 0.002[b]	SMG	$\mu = 2.5$[b]
Q0957+561A[c]	10:01:20.88	+55:53:54.0[d]	1.4141[c]	QSO	$\mu = 1.6, 1.7$[d]
Q0957+561B[c]	10:01:21.01	+55:53:49.4[d]			$\mu = 4.3$[d]
HR10[e]	16:45:02.26	+46:26:26.5[f]	1.439 ± 0.001[f]	ERO	?
IRAS F10214[g]	10:24:34.56	+47:09:09.8[h]	2.28581 ± 0.00005[h]	QSO	$\mu = 17$[h]
SMM J16371[b]	16:37:06.50	+40:53:13.8[b]	2.380 ± 0.004[b]	SMG	?
SMM J16368[i]	16:36:50.43	+40:57:34.7[i]	2.3853 ± 0.0014[i]	SMG	?
53W002[j]	17:14:14.71	+50:15:30.6[k]	2.3927 ± 0.0003[k]	Radio	Unlikely
SMM J16366[b]	16:36:58.23	+41:05:23.7[b]	2.450 ± 0.002[b]	SMG	?
SMM J04431[i]	04:43:07.25	+02:10:23.3[i]	2.5094 ± 0.0002[i]	SMG	$\mu = 4.4$[l]
SMM J16359A[m]	16:35:54.81	+66:12:37[m]	2.5168 ± 0.0003[m]	SMG	$\mu = 14$[n]
SMM J16359B[m]	16:35:44.15	+66:12:24[m]	2.5168 ± 0.0003[m]	SMG	$\mu = 22$[n]
SMM J16359C[m]	16:35:50.85	+66:12:06[m]	2.5168 ± 0.0003[m]	SMG	$\mu = 9$[n]
Cloverleaf [o]	14:15:45.97	+11:29:43.2[p]	2.5579 ± 0.0001[q]	QSO	$\mu = 11$[r]

(*Continued*)

APPENDIX 1 (*Continued*)

EMG[a]	CO coordinates R.A. (2000)	CO coordinates Decl. (2000)	Redshift z(CO)	Galaxy type	Lensed? (μ = mag.)
SMM J14011[s]	14:01:04.93	+02:52:24.1[t]	2.5652 ± 0.0001[t]	SMG	μ = 5–25[t]
VCV J1409[u]	14:09:55.50	+56:28:27.0[v]	2.5832 ± 0.0001[v]	QSO	?
LBQS 0018[z]	00:21:27.30	−02:03:33.0[u]	2.620[z]	QSO	?
MG 0414[w]	04:15:10.73	+05:34:41.2[x]	2.639 ± 0.002[w]	QSO	Yes[x]
MS1512 cB58[y]	14:14:22.22	+36:36:24.8[y]	2.7265 ± 0.0005[y]	LBG	μ = 32[y]
LBQS 1230[aa]	12:33:10.47	+16:10:53.1[bb]	2.741 ± 0.001[aa]	QSO	?
RX J0911.4[u]	09:11:27.50	+05:50:52.0[u]	2.796 ± 0.001[u]	QSO	μ = 22[cc]
SMM J02399[dd]	02:39:51.89	−01:35:58.8[ee]	2.8076 ± 0.0002[ee]	SMG	μ = 2.5[ee]
SMM J04135[u]	04:13:27.50	+10:27:40.3[u]	2.846 ± 0.002[u]	QSO	μ = 1.3[ff]
B3 J2330[gg]	23:30:24.84	+39:27:12.2[gg]	3.092[gg]	Radio	Unlikely
SMM J22174[b]	22:17:35.20	+00:15:37.6[b]	3.099 ± 0.004[b]	SMG	?
MG 0751[hh]	07:51:41.46	+27:16:31.4[hh]	3.200[hh]	QSO	μ = 17[hh]
SMM J09431[i]	09:43:03.74	+47:00:15.3[i]	3.3460 ± 0.0001[i]	SMG	μ = 1.2[ii]
SMM J13120[b]	13:12:01.20	+42:42:08.8[b]	3.408 ± 0.002[b]	SMG	?
TN J0121[jj]	01:21:42.75	+13:20:58.0[jj]	3.520[jj]	Radio	?
6C1908[kk]	19:08:23.70	+72:20:11.8[kk]	3.532[kk]	Radio	Unlikely
4C60.07[kk]	05:12:54.75	+60:30:50.9[ll]	3.791[kk]	Radio	Unlikely
4C41.17R[mm]	06:50:52.24	+41:30:31.6[mm]	3.7958 ± 0.0004[mm]	Radio	Unlikely
4C41.17B[mm]	06:50:52.12	+41:30:30.3[mm]	3.7888 ± 0.0008[mm]		
APM 08279[nn]	08:31:41.70	+52:45:17.4[nn]	3.9114 ± 0.0002[nn]	QSO	μ = 7[oo]
PSS J2322[pp]	23:22:07.15	+19:44:22.5[qq]	4.1192 ± 0.0004[qq]	QSO	μ = 2.5[rr]
BRI 1335N[ss]	13.38.03.42	−04:32:34.1[tt]	4.4074 ± 0.0015[uu]	QSO	?
BRI 1335S[ss]	13:38:03.40	−04:32:35.4[tt]	4.407[tt]		
BRI 0952[aa]	09:55:00.10	−01:30:07.1[aa]	4.4337 ± 0.0003[aa]	QSO	μ = 4[aa]
BR 1202N[vv]	12:05:22.98	−07:42:29.9[tt]	4.6916[tt]	QSO	Likely
BR 1202S[vv]	12:05:23.12	−07:42:32.9[tt]	4.6947[tt]		
TN J0924[yy]	09:24:19.92	−22:01:41.5[yy]	5.203[yy]	Radio	Unlikely
SDSS J1148[ww]	11:48:16.64	+52:51:50.3[ww]	6.4189 ± 0.0006[xx]	QSO	Yes

[a]Reference is to discovery paper; [b]Greve et al. (2005); [c]Planesas et al. (1999); [d]Krips et al. (2003); [e]Andreani et al. (2000); [f]Greve, Ivison & Papadopoulos (2003); [g]Brown & Vanden Bout (1991), Solomon, Downes & Radford (1992a); [h]Downes & Solomon (2004); [i]Neri et al. (2003); [j]Scoville et al. (1997); [k]Alloin, Barvainis & Guilloteau (2000); [l]Smail et al. (1999); [m]Sheth et al. (2004); [n]Kneib et al. (2004b); [o]Barvainis et al. (1994); [p]Center of four lensed components, Kneib et al. (1998); [q]Barvainis et al. (1997); [r]Venturini & Solomon (2003); [s]Frayer et al. (1999); [t]Downes & Solomon (2003); [u]Hainline et al. (2004); [v]Beelen et al. (2004); [w]Barvainis et al. (1998); [x]Hewitt et al. (1992); [y]Baker et al. (2004); [z]K Izaak, public communication; [aa]Guilloteau et al. (1999); [bb]Hewett et al. (1995); [cc]Barvainis & Ivison (2002); [dd]Frayer et al. (1998); [ee]Genzel et al. (2003); [ff]Knudsen et al. (2003); [gg]De Breuck et al. (2003b); [hh]Barvainis, Alloin & Bremer (2002); [ii]Cowie, Barger & Kneib (2002); [jj]De Breuck, Neri & Omont (2003a); [kk]Papadopoulos et al. (2000); [ll]Greve, Ivison & Papadopoulos (2004); [mm]De Breuck et al. (2004); [nn]Downes et al. (1999); [oo]Lewis et al. (2002); [pp]Cox et al. (2002); [qq]Carilli et al. (2002a); [rr]Carilli et al. (2003); [ss]Guilloteau et al. (1997); [tt]Carilli et al. (2002b); [uu]Carilli, Menten & Yun (1999); [vv]Omont et al. (1996b) and Ohta et al. (1995); [ww]Walter et al. (2003); [xx]Bertoldi et al.; [YY]Klamer et al. (2005).

APPENDIX 2 EMG line luminosities and molecular gas masses

EMG	Transition	$S\Delta v$ (Jy km s^{-1})	Δv (km s^{-1})	S(peak) (mJy)	L'(app.) (10^{10} L$'_*$)[a]	L'(int.) (10^{10} L$'_*$)[a]	M_{gas} (10^{10} $M_\odot$)
SMM J02396	CO(2–1)[b]	3.4 ± 0.3	780 ± 60	∼5	5.1 ± 0.5	2.0	1.6
Q0957 + 561A(r)	CO(2–1)[c]	0.34 ± 0.06	160 ± 20	2.1 ± 0.2	0.9 ± 0.2	0.6	
Q0957 + 561A(b)	CO(2–1)[c]	0.25 ± 0.06	280 ± 60	0.9 ± 0.2	0.7 ± 0.2	0.4	0.4
Q0957 + 561B	CO(2–1)[c]	0.61 ± 0.06	280 ± 50	2.2 ± 0.2	1.6 ± 0.2	0.4	
HR10	CO(1–0)[d]	0.6 ± 0.1	—	∼0.7	6.5 ± 1.1	—	5.2 μ^{-1}
	CO(2–1)[e]	1.45	400	∼4	3.8	—	
	CO(5–4)[e]	1.35	380	∼7	0.6	—	
IRAS F10214	CO(3–2)[f]	4.1 ± 0.6	220 ± 20	14.5 ± 1.5	11.3 ± 1.7	0.7	0.6
	CO(4–3)[f]	5.5 ± 1.0	220 ± 40	23 ± 4	8.6 ± 0.16	0.5	
	CO(6–5)[f]	8.5 ± 2.0	200 ± 30	32 ± 6	5.9 ± 1.4	0.4	
	CO(7–6)[f]	7.1 ± 2.0	210 ± 40	19 ± 5	3.6 ± 1.0	0.2	
	HCN(1–0)[g]	0.05 ± 0.01	140 ± 30	0.45 ± 0.08	2.3 ± 0.4	0.14	1.0
	[CI](1–0)[h]	1.6 ± 0.2	160 ± 30	9.2 ± 1.0	2.1 ± 0.3	—	
SMM J16371	CO(3–2)[b]	1.0 ± 0.2	830 ± 130	∼1	3.0 ± 0.6	—	2.4 μ^{-1}
SMM J16368	CO(3–2)[i]	2.3 ± 0.2	840 ± 110	∼3	6.9 ± 0.6	—	5.5 μ^{-1}
53W002	CO(3–2)[j]	1.20 ± 0.15	420 ± 40	2.5 ± 0.8	3.6 ± 0.4	3.6	2.9
SMM J16366	CO(3–2)[b]	1.8 ± 0.3	870 ± 80	∼2	5.6 ± 0.9	—	4.5 μ^{-1}
SMM J04431	CO(3–2)[i]	1.4 ± 0.2	350 ± 60	3.5 ± 0.5	4.5 ± 0.6	1.0	0.8
SMM J16359A	CO(3–2)[k]	1.67 ± 0.13	∼500	∼4	5.5 ± 0.4	0.4	
SMM J16359B	CO(3–2)[k]	2.50 ± 0.12	∼500	∼7	8.2 ± 0.4	0.4	0.4
SMM J16359C	CO(3–2)[k]	1.58 ± 0.17	∼500	∼4	5.2 ± 0.6	0.6	

(*Continued*)

APPENDIX 2 (*Continued*)

EMG	Transition	$S\Delta v$ (Jy km s^{-1})	Δv (km s^{-1})	S (peak) (mJy)	L'(app.) (10^{10} L$'_*$)[a]	L'(int.) (10^{10} L$'_*$)[a]	M_{gas} (10^{10} $M_\odot$)
Cloverleaf	CO(3–2)[l]	13.2 ± 0.2	416 ± 6	30.0 ± 1.7	44 ± 1	4.0	3.2
	CO(4–3)[m]	21.1 ± 0.8	375 ± 16	53 ± 2	40 ± 2	3.6	
	CO(5–4)[m]	24.0 ± 1.4	398 ± 25	56 ± 3	29 ± 2	2.6	
	CO(7–6)[n]	36 ± 6	∼450	80 ± 8	22 ± 4	2.0	
	HCN(1–0)[o]	0.069 ± 0.012	∼300	0.24 ± 0.04	3.5 ± 0.6	0.32	2.2
	[CI](1–0)[h]	3.9 ± 0.6	360 ± 60	11.2 ± 2.0	6.5 ± 1.0	—	
	[CI](2–1)[l]	5.2 ± 0.3	468 ± 25	13.2 ± 2.9	3.2 ± 0.2	—	
SMM J14011	CO(3–2)[p]	2.8 ± 0.3	190 ± 11	13.2 ± 1.0	9.4 ± 1.0	0.4–1.9	0.3–1.5
	CO(7–6)[p]	3.2 ± 0.5	170 ± 30	12.4 ± 3.0	2.0 ± 0.3	0.08–0.4	
	[CI](1–0)[h]	1.8 ± 0.3	235 ± 45	7.3 ± 1.5	3.0 ± 0.5	—	
VCV J1409	CO(3–2)[q]	2.3 ± 0.2	311 ± 28	6 ± 1	7.9 ± 0.7	—	$6.3\,\mu^{-1}$
	CO(7–6)[q]	4.1 ± 1.0	∼300	10 ± 3	2.6 ± 0.6	—	
	HCN(1–0)[r]	0.007 ± 0.002	∼200	0.08 ± 0.03	0.7 ± 0.2	—	$4.9\,\mu^{-1}$
LBQS 0018	CO(3–2)[s]	1.55 ± 0.26	163 ± 29	—	5.4 ± 0.9	—	$4.3\,\mu^{-1}$
MG0414	CO(3–2)[t]	2.6 ± 0.5	∼580	4.4	9.2	—	$7.4\,\mu^{-1}$
MS1512 − cB58	CO(3–2)[u]	0.37 ± 0.08	175 ± 45	∼2	1.4 ± 0.3	0.043	0.03
LBQS 1230	CO(3–2)[v]	0.80 ± 0.26	—	—	3.0 ± 1.0	—	$2.4\,\mu^{-1}$
RX J0911.4	CO(3–2)[w]	2.9 ± 1.1	350 ± 60	∼8	11.3 ± 4.3	0.52	0.4
SMM J02399	CO(3–2)[x]	3.1 ± 0.4	∼1100	∼4	12.2 ± 1.6	4.9	3.9

SMM J04135	CO(3–2)[w]	5.4 ± 1.3	340 ± 120	∼16	22 ± 5	17	13
B3 J2330	CO(4–3)[y]	1.3 ± 0.3	∼500	2.5	3.4 ± 0.8	3.4	2.7
SMM J22174	CO(3–2)[b]	0.8 ± 0.2	780 ± 100	∼1	3.7 ± 0.9	—	3.0
MG0751	CO(4–3)[z]	5.96 ± 0.45	390 ± 40	∼15	16 ± 1	1.0	0.8
SMM J09431	CO(4–3)[i]	1.1 ± 0.1	420 ± 50	2.5 ± 0.5	3.2 ± 0.3	2.7	2.2
SMM J13120	CO(4–3)[b]	1.7 ± 0.3	530 ± 50	∼3	5.2 ± 0.9	—	4.2 μ^{-1}
TN J0121	CO(4–3)[aa]	1.2 ± 0.4	∼700	∼2	5.4 ± 1.0	5.4	4.3
6C1908	CO(4–3)[bb]	1.62 ± 0.30	530 ± 70	∼3	5.2 ± 1.0	5.2	4.2
4C60.07	CO(1–0)[cc]	0.15 ± 0.03	∼550	0.27 ± 0.05	8.7 ± 1.7	8.7	7.0
	CO(1–0)[cc]	0.09 ± 0.01	165 ± 24	0.30 ± 0.10	5.2 ± 0.6	5.2	4.2
	CO(4–3)[bb]	1.65 ± 0.35	∼550	∼3	6.0 ± 0.9	6.0	
	CO(4–3)[bb]	0.85 ± 0.2	∼150	∼6	3.0 ± 0.2	3.0	
4C41.17R	CO(4–3)[dd]	1.20 ± 0.15	500 ± 100	∼2.5	4.3 ± 0.5	4.3	5.2
4C41.17B	CO(4–3)[dd]	0.60 ± 0.15	500 ± 150	∼1.5	2.2 ± 0.5	2.2	
APM 08279	CO(1–0)[ee]	0.150 ± 0.045	—	—	9.1 ± 2.7	1.3	1.0
	CO(4–3)[ff]	3.7 ± 0.5	480 ± 35	7.4 ± 1.0	14 ± 2	2.0	
	CO(9–8)[ff]	9.1 ± 0.8	∼500	17.9 ± 1.4	6.8 ± 0.6	1.0	
(N/NE comp.)[gg]	CO(2–1)[ee]	1.15 ± 0.54	—	—	17 ± 8	—	
PSS J2322	CO(1–0)[hh]	0.19 ± 0.08	200 ± 70	0.9 ± 0.2	12 ± 5	5.0	4.0
	CO(2–1)[hh]	0.92 ± 0.30	—	2.70 ± 0.24	15 ± 5	6.1	
	CO(4–3)[ii]	4.21 ± 0.40	375 ± 40	10.5	17.3 ± 1.6	6.9	
	CO(5–4)[ii]	3.74 ± 0.56	275 ± 50	12	9.8 ± 1.5	3.9	
	[CI](1–0)[jj]	0.81 ± 0.12	319 ± 66	2.4	3.3 ± 0.5	—	

(*Continued*)

APPENDIX 2 (*Continued*)

EMG	Transition	$S\Delta v$ (Jy km s^{-1})	Δv (km s^{-1})	S (peak) (mJy)	L'(app.) (10^{10} L$'_*$)[a]	L'(int.) (10^{10} L$'_*$)[a]	M_{gas} (10^{10} $M_\odot$)
BRI 1335N	CO(2–1)[kk]	0.18 ± 0.06	—	0.45 ± 0.14	3.3 ± 1.1	—	2.6 μ^{-1}
BRI 1335S	CO(2–1)[kk]	0.26 ± 0.06	—	0.67 ± 0.14	4.8 ± 1.1	—	3.8 μ^{-1}
BRI 1335	CO(5–4)[ll]	2.8 ± 0.3	420 ± 60	6 ± 1	8.2 ± 0.9	—	6.6 μ^{-1}
BRI 0952	CO(5–4)[v]	0.91 ± 0.11	230	∼3	2.8 ± 0.3	0.7	0.5
BR 1202N	CO(2–1)[kk]	0.26 ± 0.05	—	0.44 ± 0.07	5.2 ± 1.0	—	4.2
	CO(5–4)[mm]	1.3 ± 0.3	∼350	∼3	4.2 ± 1.0	—	
BR 1202S	CO(2–1)[kk]	0.23 ± 0.04	—	0.77 ± 0.10	4.6 ± 0.8	—	3.7
	CO(5–4)[mm]	1.1 ± 0.2	∼190	∼5	3.5 ± 0.6	—	
BR 1202	CO(4–3)[mm]	1.5 ± 0.3	—	—	7.6 ± 1.5	—	6.1
	CO(7–6)[mm]	3.1 ± 0.9	∼275	∼10	5.1 ± 1.5	—	
TN J0924	CO(1–0)	0.087 ± 0.017	∼300	0.52 ± 0.12	8.2 ± 1.6	8.2	6.6
	CO(5–4)	1.19 ± 0.27	∼300	7.8 ± 2.7	4.5 ± 1.0	4.5	
SDSS J1148	CO(3–2)[nn]	0.18 ± 0.04	∼250	∼0.6	2.6 ± 0.6	—	2.1
	CO(6–5)[oo]	0.73 ± 0.076	∼280	∼2.5	2.6 ± 0.3	—	
	CO(7–6)[oo]	0.640 ± 0.088	∼280	∼2.1	1.7 ± 0.2	—	

[a]L$'_*$ = K km s^{-1} pc^2; [b]Greve et al. (2005); [c]Krips et al. (2003); [d]Greve, Ivison & Papadopoulos (2003); [e]Andreani et al. (2000); [f]D Downes & PM Solomon, manuscript in preparation; [g]Vanden Bout, Solomon & Maddalena (2004); [h]Weiß et al. (2005); [i]Neri et al. (2003); [j]Alloin, Barvainis & Guilloteau (2000); [k]Kneib et al. (2004a); [l]Weiß et al. (2003); [m]Barvainis et al. (1997); [n]Kneib et al. (1998); [o]Solomon et al. (2003); [p]Downes & Solomon (2003); [q]Beelen et al. (2004); [r]Carilli et al. (2004); [s]K Izaak, private communication; [t]Barvainis et al. (1998); [u]Baker et al. (2004); [v]Guilloteau et al. (1999); [w]Hainline et al. (2004); [x]Genzel et al. (2003); [y]De Breuck et al. (2003a); [z]Barvainis, Alloin & Bremer (2002); [aa]De Breuck et al. (2003b); [bb]Papadopoulos et al. (2000); [cc]Greve, Ivison & Papadopoulos (2004); [dd]De Breuck et al. (2004); [ee]Papadopoulos et al. (2001); [ff]Downes et al. (1999); [gg]Components lie 2–3″ to N and NE and may be unrelated to the nuclear source; [hh]Carilli et al. (2002a); [ii]Cox et al. (2002); [jj]Pety et al. (2004); [kk]Carilli et al. (2002b); [ll]Guilloteau et al. (1997); [mm]Omont et al. (1996b); [nn]Walter et al. (2003); [oo]Bertoldi et al. (2003b).

APPENDIX 3 EMG FIR luminosities and dust masses

EMG	Band (μm)	Flux density (mJy)	L_{FIR}(app.) ($10^{12}\,L_\odot$)	L_{FIR}(int.) ($10^{12}\,L_\odot$)	M_{dust} ($10^{8}\,M_\odot$)
SMM02396	850[a]	11	16.3[a]	6.5[a]	
	450[a]	42			
Q0957 + 561	850[b]	7.5 ± 1.4	14[c]	6[c]	2.5[b]
HR10	1350[d]	2.13 ± 0.63			
	850[d]	4.89 ± 0.74	6.5[d]		$6.8\mu^{-1}$[d]
	450[d]	32.3 ± 8.5			
	850[e]	8 ± 2	9[e]		$9\mu^{-1}$[e]
IRAS F10214	1410[f]	5.7 ± 1.0			0.23[f]
	1240[f]	10 ± 2			
	1230[g]	9.6 ± 1.4			
	1100[h]	24 ± 5	60[f]	3.6[f]	
	850[h]	50 ± 5			
	450[i]	273 ± 45			
	350[j]	383 ± 51			
SMM J16371	1300[k]	4.2 ± 1.1			
	850[l]	11.2 ± 2.9			
SMM J16368	1300[m]	2.5 ± 0.4			
	850[n]	8.2 ± 1.7	16[c]		
53W002	1300[o]	1.7 ± 0.4			
SMM J16366	850[n]	10.7 ± 2.0	20[c]		
SMM J04431	1300[l]	1.1 ± 0.3			
	850[p]	7.2 ± 1.7	13[m]	3[m]	
SMM J16359	1350[q]	3.0 ± 0.7			
SMM J16359A	850[r]	11 ± 1			
	450[r]	45 ± 9			
SMM J16359B	850[r]	17 ± 2	45[r]	1[r]	2[s]
	450[r]	75 ± 15			
SMM J16359C	850[r]	9 ± 1			
	450[r]	32 ± 6			
Cloverleaf	1300[b]	18 ± 2			
	850[b]	58.8 ± 8.1	59[t]	5.4[t]	1.5[t]
	450[b]	224 ± 38			
	350[j]	293 ± 14	77[j]	7[j]	3.5[j]
SMM J14011	1350[u]	2.5 ± 0.8	20[u]	0.8–4.0[u]	0.13–0.65[v]
	850[w]	14.6 ± 1.8			
	450[w]	41.9 ± 6.9			

(*Continued*)

APPENDIX 3 (*Continued*)

EMG	Band (μm)	Flux density (mJy)	L_{FIR}(app.) ($10^{12}\,L_\odot$)	L_{FIR}(int.) ($10^{12}\,L_\odot$)	M_{dust} ($10^8\,M_\odot$)
VCV J1409	1300[x]	10.7 ± 0.6	43[x]		
	350[y]	159 ± 14[y]	35[y]		$38\mu^{-1}$[x]
LBQS 0018	850[z]	17.2 ± 2.9	33[c]		
MG0414	3000[b]	40 ± 2			
	1300[b]	20.7 ± 1.3			
	850[b]	16.7 ± 3.8	32[c]		
	450[b]	66 ± 16			
MS1512 − cB58	1200[aa]	1.06 ± 0.35			
	850[bb]	4.2 ± 0.9	3.1[bb]	0.1[bb]	
LBQS 1230	1350[cc]	3.3 ± 0.5			
	1250[cc]	7.5 ± 1.4			
	350[j]	104 ± 21	36[j]		$11\mu^{-1}$[j]
RX J0911.4	3000[b]	1.7 ± 0.3			
	1300[b]	10.2 ± 1.8			
	850[b]	26.7 ± 1.4	51[c]	2.3[c]	
	450[b]	65 ± 19			
	350[dd]	∼50			
SMM J02399	1270[ee]	7.0 ± 1.2			
	1350[ff]	5.7 ± 1.0	11[ff]	4.4[ff]	6−8[ff]
	850[f]	26 ± 3			
	750[ff]	28 ± 5			
	450[ff]	69 ± 15			
SMM J04135	850[gg]	25.0 ± 2.8	31[gg]	24[gg]	18[gg]
	450[gg]	55 ± 17			
B3 J2330	1200[hh]	4.8 ± 1.2	28[hh]	28[hh]	
	850[ii]	14.1 ± 1.7	13[hh]	13[ii]	
	450[ii]	49 ± 18			
SMM J22174	850[l]	6.3 ± 1.3	12[c]		
MG0751	3000[ij]	4.1 ± 0.5			
	1300[ij]	6.7 ± 1.3			
	850[b]	25.8 ± 1.3	49[c]	2.9[c]	
	450[b]	71 ± 15			
SMM J09431	1300[m]	2.3 ± 0.4			
	850[kk]	10.5 ± 1.8	20[m]	17[m]	
SMM J13120	850[ll]	6.2 ± 1.2	12[c]		
TN J0121	850[ii]	7.5 ± 1.0	7[ii]	7[ii]	

(*Continued*)

APPENDIX 3 (*Continued*)

EMG	Band (μm)	Flux density (mJy)	L_{FIR}(app.) ($10^{12}\,L_\odot$)	L_{FIR}(int.) ($10^{12}\,L_\odot$)	M_{dust} ($10^{8}\,M_\odot$)
6C1908	850[ii]	10.8 ± 1.2	9.8[ii]	9.8[ii]	
4C60.07	1250[mm]	4.5 ± 1.2			
	850[ii]	14.4 ± 1.0	13[ii]	13[ii]	
	850[nn]	17.1 ± 1.3	32[c]		
	450[nn]	69 ± 23			
4C41.17	1245[oo]	3.4 ± 0.7			
	850[nn]	12.1 ± 0.9			
	450[nn]	22.5 ± 8.5			
	350[j]	37 ± 9	20[j]	20[j]	4.6[j]
APM 08279	3200[pp]	1.2 ± 0.3			
	1400[pp]	17.0 ± 0.5			
	1300[b]	24 ± 2			
	850[b]	84 ± 3			
	450[b]	285 ± 11			
	350[y]	392 ± 36	200[y]	29[y]	5.8[y]
PSS J2322	1200[qq]	9.6 ± 0.5			9.0[qq]
	1350[rr]	7.5 ± 1.3	23[rr]	9.3[rr]	
	850[rr]	24 ± 2			
	450[rr]	79 ± 19			
	350[y]	66 ± 9	30[y]	12[y]	9.6[y]
BRI 1335	1350[cc]	5.6 ± 1.1			
	1250[cc]	10.3 ± 1.4			
	350[j]	52 ± 8	28[j]		$17\mu^{-1}$[j]
BRI 0952	1350[cc]	2.2 ± 0.5	9.6[cc]	2.4[cc]	0.7[cc]
	1250[cc]	2.78 ± 0.63			
	850[b]	13.4 ± 2.3	25[c]	6.4[c]	
BR 1202	1350[cc]	16 ± 2			
	350[j]	106 ± 7	71[j]		19[j]
SDSS J1148	1200[ss]	5.0 ± 0.6	25[tt]		6.7 μ^{-1}[ss]
	850[tt]	7.8 ± 0.7			2.8 μ^{-1}[tt]
	450[tt]	24.7 ± 7.4			
	350[y]	23 ± 3	27[y]		4.4 μ^{-1}[y]

[a]Smail et al. (2002); [b]Barvainis & Ivison (2002); [c]Using $L_{FIR} = 1.9 \times 10^{12} S_{850}$, Neri et al. (2003); [d]Dey et al. (1999); [e]Greve, Ivison & Papadopoulos (1999); [f]D Downes & PM Solomon, mansucript in preparation; [g]Downes et al. (1992); [h]Rowan-Robinson et al. (1993); [i]Clements et al. (1992); [j]Benford et al. (1999); [k]Greve et al. (2004); [l]Chapman et al. (2005); [m]Neri et al. (2003); [n]Ivison et al. (2002); [o]Alloin, Barvainis & Guilloteau (2000); [p]Smail et al. (1999); [q]Kneib et al. (2004a); [r]Kneib et al. (2004b); [s]Sheth et al. (2004); [t]Weiß et al. (2003); [u]Downes & Solomon (2003); [v]Mean for μ = 5–25, Downes & Solomon (2003); [w]Ivison et al. (2000); [x]Omont et al. (2003); [y]A Beelen, P Cox, DJ Benford, CD Dowell, A Kovacs, et al., in preparation; [z]Priddey et al. (2003); [aa]Baker et al. (2001); [bb]van der Werf et al. (2001); [cc]Guilloteau et al. (1999); [dd]J-W Wu, private communication; [ee]Genzel et al. (2003); [ff]Ivison et al. (1998); [gg]Knudsen, van der Werf & Jaffe (2003); [hh]De Breuck et al. (2003a); [ii]Reuland et al. (2004); [jj]Barvainis, Alloin & Bremer (2002); [kk]Cowie, Barger & Kneib (2002); [ll]Chapman et al. (2003); [mm]Papadopoulos et al. (2000); [nn]Archibald et al. (2001); [oo]De Breuck et al. (2004); [pp]Downes et al. (1999); [qq]Omont et al. (2001); [rr]Cox et al. (2002); [ss]Bertoldi et al. (2003a); [tt]Robson et al. (2004).

The *Annual Review of Astronomy and Astrophysics* is online at http://astro.annualreviews.org

LITERATURE CITED

Alexander DM, Bauer FE, Chapman SC, Smail I, Blain AW, et al. 2004. *Proc. ESO/ USM/MPE Workshop Multiwavel. Mapping Galaxy Form. Evol.*, ed. R Bender, A Renzini, pp. 58–61. Springer: Berlin

Alloin D, Barvainis R, Guilloteau S. 2000. *Astrophys. J.* 528:L81–84

Alloin D, Guilloteau S, Barvainis R, Antonucci R, Tacconi L. 1997. *Astron. Astrophys.* 321:24–28

Andreani P, Cimatti A, Loinard L, Röttgering RJA. 2000. *Astron. Astrophys.* 354:L1–5

Archibald EN, Dunlop JS, Hughes DH, Rawlings S, Eales SA, Ivison RJ. 2001. *MNRAS* 323:417–44

Baker AJ, Lutz D, Genzel R, Tacconi LJ, Lehnert MD. 2001. *Astron. Astrophys.* 372:L37–40

Baker AJ, Tacconi LJ, Genzel R, Lehnert MD, Lutz D. 2004. *Astrophys. J.* 604:125–40

Barvainis R, Alloin D, Bremer M. 2002. *Astron. Astrophys.* 385:399–403

Barvainis R, Alloin D, Guilloteau S, Antonucci R. 1998. *Astrophys. J.* 492:L13–16

Barvainis R, Antonucci R, Coleman P. 1992. *Astrophys. J.* 399:L19–22

Barvainis R, Ivison R. 2002. *Astrophys. J.* 571:712–20

Barvainis R, Maloney P, Antonucci R, Alloin D. 1997. *Astrophys. J.* 484:695–701

Barvainis R, Tacconi L, Antonucci R, Alloin D, Coleman P. 1994. *Nature* 371:586–88

Beelen A, Cox P, Pety J, Carilli CL, Bertoldi F, et al. 2004. *Astron. Astrophys.* 423:441–47

Benford DJ, Cox P, Omont A, Phillips TG, McMahon RG. 1999. *Astrophys. J.* 518:L65–68

Bertoldi F, Carilli CL, Cox P, Fan X, Strauss MA, et al. 2003a. *Astron. Astrophys.* 406:L55–58

Bertoldi F, Cox P, Neri R, Carilli C, Walter F, et al. 2003. *Astron. Astrophys.* 409:L47–50

Blain A. 2001. In *Proc. Symp. Sci. Atacama Large Millimeter Array, Washington, DC, 6–8 Oct. 1999*, *Astron. Soc. Pac. Conf. Ser.*, ed. A Wootten, 235:261–70

Bloemen JBGM, Strong AW, Mayer-Hasselwander HA, Blitz L, Cohen RS, et al. 1986. *Astron. Astrophys.* 154:25–41

Bolatto AD, Di Francesco J, Willott CJ. 2004. *Astrophys. J.* 606:L101–3

Broadhurst T, Leh'ar J. 1995. *Astrophys. J.* 450:L41–44

Brown RL, Vanden Bout PA. 1991. *Astron. J.* 102:1956–59

Brown RL, Vanden Bout PA. 1992. *Astrophys. J.* 397:L19–22

Carilli CL, Cox P, Bertoldi F, Menten KM, Omont A, et al. 2002a. *Astrophys. J.* 575: 145–49

Carilli CL, Kohno K, Kawabe R, Ohta K, Henkel C, et al. 2002b. *Astron. J.* 123:1838–46

Carilli CL, Lewis GF, Djorgovski SG, Mahabal A, Cox P, et al. 2003. *Science* 300:773–75

Carilli CL, Menten KM, Yun MS. 1999. *Astrophys. J.* 521:L25–28

Carilli CL, Solomon P, Vanden Bout P, Walter F, Beelen A, et al. 2004. *Astrophys. J.* 618:586–91

Chapman SC, Blain AW, Ivison RJ, Smail I. 2003. *Nature* 422:695–98

Chapman SC, Blain AW, Smail I, Ivison RJ. 2005. *Astrophys. J.* 622:772–96

Chapman SC, Smail I, Windhorst R, Muxlow T, Ivison RJ. 2004. *Astrophys. J.* 611:732–38

Clements DL, Rowan-Robinson M, Lawrence A, Broadhurst T, McMahon R. 1992. *MNRAS* 256:P35–37

Cowie LL, Barger AJ, Kneib J-P. 2002. *Astron. J.* 123:2197–205

Cox P, Omont A, Djorgovski SG, Bertoldi F, Pety J, et al. 2002. *Astron. Astrophys.* 387: 406–11

Davies RI, Tacconi LJ, Genzel R. 2004. *Astrophys. J.* 731:781–93

De Breuck C, Neri R, Downes D, van Breugel W, Reuland M, et al. 2005. *Astron. Astrophys.* 430:L1–4

De Breuck C, Neri R, Morganti R, Omont A, Rocca-Volmerange B, et al. 2003. *Astron. Astrophys.* 401:911–25

De Breuck C, Neri R, Omont A. 2003b. *New Astron. Rev.* 47:285–89

Dey A, Graham JR, Ivison RJ, Smail I, Wright GS, Liu MC. 1999. *Astrophys. J.* 519:610–21

Dickman RL. 1978. *Astrophys. J. Suppl.* 37: 407–27

Dickman RL, Snell R, Schloerb P. 1987. *Astrophys. J.* 309:326–30

Downes D, Neri R, Wiklind T, Wilner DJ, Shaver PA. 1999. *Astrophys. J.* 513:L1–L4

Downes D, Radford SJE, Greve A, Thum C, Solomon PM, Wink JE. 1992. *Astrophys. J.* 398:L25–27

Downes D, Solomon PM, Radford SJE. 1993. *Astrophys. J.* 414:L13–16

Downes D, Solomon PM, Radford SJE. 1995. *Astrophys. J.* 453:L65–68

Downes D, Solomon PM. 1998. *Astrophys. J.* 507:615–54

Downes D, Solomon PM. 2003. *Astrophys. J.* 582:37–48

Egami E, Neugebauer G, Soifer BT, Matthews K, Ressler M, et al. 2000. *Astrophys. J.* 535:561–74

Frayer DT, Ivison RJ, Scoville NZ, Evans AS, Yun MS, et al. 1999. *Astrophys. J.* 514:L13–16

Frayer DT, Ivison RJ, Scoville NZ, Yun M, Evans AS, et al. 1998. *Astrophys. J.* 506:L7–10

Gao Y, Solomon PM. 2004. *Astrophys. J.* 606: 271–90

Genzel R, Baker AJ, Ivison RJ, Bertoldi F, Blain AW, et al. 2004. *Proc. ESO/USM/MPE Workshop Multiwavel. Mapping Galaxy Form. Evol.*, ed. R Bender, A Renzini, pp. 112–15. Springer: Berlin

Genzel R, Baker AJ, Tacconi LJ, Lutz D, Cox P, et al. 2003. *Astrophys. J.* 584:633–42

Gerin M, Phillips TJ. 2000. *Astrophys. J.* 537: 644–53

Giavalisco M. 2002. *Annu. Rev. Astron. Astrophys.* 40:579–641

Goldreich P, Kwan J. 1974. *Astrophys. J.* 537:644–53

Goodrich RW, Miller JS, Martei A, Cohen MH, Tran HD, et al. 1996. *Astrophys. J.* 56:L9–12

Graham JR, Liu MC. 1995. *Astrophys. J.* 449:L29–32

Greve TR, Bertoldi F, Smail I, Neri R, Chapman SC, et al. 2005. *MNRAS.* 359:1165–83

Greve TR, Ivison RJ, Bertoldi F, Stevens JA, Dunlop JS, et al. 2004. *MNRAS* 354:779–97

Greve TR, Ivison RJ, Papadopoulos PP. 2003. *Astrophys. J.* 599:839–46

Greve TR, Ivison RJ, Papadopoulos PP. 2004. *Astron. Astrophys.* 419:99–107

Guilloteau S. 2001. In *Proc. Symp. Sci. Atacama Large Millimeter Array, Washington, DC, 6–8 Oct. 1999, Astron. Soc. Pac. Conf. Ser.*, ed. A Wootten, 235:271–79

Guilloteau S, Omont A, Cox P, McMahon RG, Petitjean P. 1999. *Astron. Astrophys.* 349:363–68

Guilloteau S, Omont A, McMahon RG, Cox P, Petitjean P. 1997. *Astron. Astrophys.* 328: L1–4

Hainline LJ, Scoville NZ, Yun MS, Hawkins DW, Frayer DT, Isaak KG. 2004. *Astrophys. J.* 609:61–68

Hazard C, Morton DC, Terlevich R, McMahon R. 1984. *Astrophys. J.* 282:33–52

Hewett PC, Foltz CB, Chaffee FH. 1995. *Astron. J.* 109:1498–521

Hewitt JN, Turner EL, Lawrence CR, Schneider DP, Brody JP. 1992. *Astron. J.* 104:968–79

Irwin MJ, Ibata RA, Lewis GF, Totlen EJ. 1998. *Astrophys. J.* 505:529–35

Ivison RJ, Greve TR, Smail I, Dunlop JS, Roche ND, et al. 2002. *MNRAS* 337:1–25

Ivison RJ, Smail I, Barger AJ, Kneib J-P, Blain AW, et al. 2000. *MNRAS* 315:209–22

Ivison RJ, Smail I, Frayer DT, Kneib J-P, Blain AW. 2001. *Astrophys. J.* 561:L45–49

Ivison RJ, Smail I, LeBorgne J-F, Blain AW, Kneib J-P, et al. 1998. *MNRAS* 298:583–93

Izaak K, Riddey RS, McMahon RG, Omont

A, Peroux C, et al. 2002. *MNRAS* 329:149–62

Kennicutt R. 1998. *Annu. Rev. Astron. Astrophys.* 36:189–231

Kneib J-P, Alloin D, Mellier Y, Guilloteau S, Barvainis R, Antonucci R. 1998. *Astron. Astrophys.* 329:827–39

Kneib J-P, Mellier Y, Fort B, Mathez G. 1993. *Astron. Astrophys.* 273:367–76

Kneib J-P, Neri R, Smail I, Blain A, Sheth K, et al. 2004a. *Astron. Astrophys.* 434:819–25

Kneib J-P, van der Werf PP, Knudsen KK, Smail I, Blain A, et al. 2004b. *MNRAS* 349: 1211–17

Knudsen KK, van derWerf PP, Jaffe W. 2003. *Astron. Astrophys.* 411:343–50

Krips M, Neri R, Martín-Pintado J, Planesas P, Colina L. 2003. *Proc. Symp. The Dense Interstellar Medium in Galaxies*, Zermatt, Switzerland, 22–26 Sept., ed. S Pfalzner, C Kramer, C Staubmeier, A Heithausen. Springer Proc. Phys. 91:23–26

Lawrence A, Rowan-Robinson M, Oliver S, Taylor A, McMahon RG, et al. 1993. *MNRAS* 260:28–36

Lewis GF, Carilli C, Papadopoulos P, Ivison RJ. 2002. *MNRAS* 330:L15–18

Magain P, Surdej J, Swings J-P, Borgeest U, Kayser R, et al. 1988. *Nature* 334:325–27

Malhotra S. 2000. *Proc. Symp. The Promise of the Herschel Space Observatory, Toledo, Spain, 12–15 Dec.* ed. GL Pilbratt, J Cernicharo, AM Heras, T Prusti, R Harris, ESA SP-460, pp. 155–58

Matthews K, Soifer BT, Nelson J, Boesgaard H, Graham JR, et al. 1994. *Astrophys. J.* 420:L13–16

Neri R, Genzel R, Ivison RJ, Bertoldi F, Blain AW, et al. 2003. *Astrophys. J.* 597:L113–16

Ohta K, Yamada T, Nakanishi K, Kohno K, Akiyama M, Kawabe R. 1995. *Nature* 382: 426–28

Ojha R, Stark A, Hsieh HH, Lane AP, Chamberlin RA, et al. 2001. *Astrophys. J.* 548:253–57

Omont A, Cox P, Berthodi F, McMahon RG, Carilli C, Isaak K. 2001. *Astron. Astrophys.* 374:371–81

Omont A, Beelen A, Bertoldi F, Cox P, Carilli C, et al. 2003. *Astron. Astrophys.* 398:857–65

Omont A, McMahon RG, Cox P, Kreysa E, Bergeron J, et al. 1996a. *Astron. Astrophys.* 315:1–10

Omont A, Petitjean P, Guilloteau S, McMahon RG, Solomon PM, Pécontal E. 1996b. *Nature* 382:428–31

Papadopoulos PP, Greve TR. 2004. *Astrophys. J.* 615:L29–32

Papadopoulos PP, Ivison R, Carilli C, Lewis G. 2001. *Nature* 409:58–60

Papadopoulos PP, Röttgering HJA, van der Werf PP, Guilloteau S, Omont A, et al. 2000. *Astrophys. J.* 528:626–36

Papadopoulos PP, Thi W-F, Viti S. 2004. *MNRAS* 351:147–60

Pety J, Beelen A, Cox P, Downes D, Omont A, et al. 2004. *Astron. Astrophys.* 428:L21–24

Planesas P, Martin-Pintado J, Neri R, Colina L. 1999. *Science* 286:2493–95

Priddey RS, Isaak KG, McMahon RG, Omont A. 2003. *MNRAS* 344:L74–78

Radford SJE, Downes D, Solomon PM, Barrett J, Sage LJ. 1996. *Astron. J.* 111:1021–24

Reuland M, Röttgering H, van Breugel W, De Breuck C. 2004. *MNRAS* 353:377–90

Robson I, Priddey RS, Isaak KG, McMahon RG. 2004. *MNRAS* 351:L29–33

Rowan-Robinson M, Broadhurst T, Lawrence A, McMahon RG, Lonsdale DJ, et al. 1991. *Nature* 351:719–21

Rowan-Robinson M, Efstathiou A, Lawrence A, Oliver S, Taylor A, et al. 1993. *MNRAS* 261:513–21

Sanders D, Mirabel IF. 1996. *Annu. Rev. Astron. Astrophys.* 34:749–92

Sanders D, Scoville NZ, Young JS, Soifer BT, Schloerb FP, et al. 1988. *Astrophys. J.* 305:L45–49

Sawicki M. 2001. *Astron. J.* 121:2405–12

Scott SE, Fox MJ, Dunlop JS, Serjeant S, Peacock JA, et al. 2002. *MNRAS* 337:817–38

Scoville NZ, Sargent AI, Sanders DB, Soifer BT. 1991. *Astrophys. J.* 366:L5–9

Scoville NZ, Solomon PM. 1974. *Astrophys. J.* 187:L67–71

Scoville NZ, Yun MS, Windhorst RA, Keel WC, Armus L. 1997. *Astrophys. J.* 485:L21–24

Sheth K, Blain AW, Kneib J-P, Frayer DT, van der Werf PP, Knudsen KK. 2004. *Astrophys. J.* 614:L5–8

Shirley YL, Evans NJ, Young KE, Knez C, Jaffe DT. 2003. *Astrophys. J. Suppl.* 149:375–403

Smail I, Ivison RJ, Blain AW. 1997. *Astrophys. J.* 490:L5–8

Smail I, Ivison RJ, Blain AW, Kneib J-P. 2002. *MNRAS* 331:495–520

Smail I, Ivison RJ, Kneib J-P, Cowie LL, Blain AW, et al. 1999. *MNRAS* 308:1061–68

Solomon PM, Barrett JW. 1991. In *Dynamics of Galaxies and Their Molecular Cloud Distributions: Proc. Symp. Int. Astron. Union*, 146th, ed. F Combes, F Casoli, pp. 235–41. Dordrecht: Kluwer

Solomon PM, Downes D, Radford SJE. 1992a. *Astrophys. J.* 398:L29–32

Solomon PM, Downes D, Radford SJE. 1992b. *Nature* 356:318–19

Solomon PM, Downes D, Radford SJE. 1992c. *Astrophys. J.* 387:L55–59

Solomon PM, Downes D, Radford SJE, Barrett JW. 1997. *Astrophys. J.* 478:144–61

Solomon PM, Rivolo AR, Barrett J, Yahil A. 1987. *Astrophys. J.* 319:730–41

Solomon PM, Sage LJ. 1988. *Astrophys. J.* 334:613–24

Solomon P, Vanden Bout P, Carilli CL, Guelin M. 2003. *Nature* 426:636–38

Solomon PM, Wickramasinghe NC. 1969. *Astrophys. J.* 158:449–60

Stevens JA, Ivison RJ, Dunlop JS, Smail I, Percival WJ, et al. 2003. *Nature* 425:264–67

Strong AW, Bloemen JBGM, Dame TM, Grenier IA, Hermsen W, et al. 1988. *Astron. Astrophys.* 207:1–15

Stutzki J, Graf UU, Haas S, Honingh CE, Hottgenroth D, et al. 1997. *Astrophys. J.* 477:L33–36

Tecza M, Baker AJ, Davies RI, Genzel R, Lehnert MD, et al. 2004. *Astrophys. J.* 605:L109–12

Vanden Bout PA, Solomon PM, Maddalena RJ. 2004. *Astrophys. J.* 614:97–100

van der Werf PP. 1999. In *Highly Redshifted Radio Lines*, ed. CL Carilli, SJE Radford, KM Menten, GI Langston. ASP Conf. Ser. 156, pp. 91–98

van der Werf PP, Knudsen KK, Labbé I, Franx M. 2000. *Proc. Symp. Deep Millimeter Surv.: Implic. Galaxy Form. Evol.*, Amherst, Mass., 19–21 June, ed. JD Lowenthal, DH Hughes. World Scientific, pp. 103–6

Venturini S, Solomon PM. 2003. *Astrophys. J.* 590:740–45

Walter F, Bertoldi F, Carilli CL, Cox P, Lo KY, et al. 2003. *Nature* 424:406–8

Walter F, Carilli C, Bertoldi F, Menten K, Cox P, et al. 2004. *Astrophys. J.* 615:L17–20

Weiß A, Downes D, Henkel D, Walter F. 2005. *Astron. Astrophys.* 429:L25–28

Weiß A, Henkel D, Downes D, Walter F. 2003. *Astron. Astrophys.* 409:L41–45

Wiklind T, Alloin D. 2002. In *Gravitational Lensing: An Astrophysical Tool*, ed. F Courbin, D Minniti. Springer Lect. Notes Phys. 608:124–88

Young JS, Schloerb FP, Kenney JD, Lord SD. 1986. *Astrophys. J.* 304:443–58

Yun M, Scoville NZ, Carrasco JJ, Blandford RD. 1997. *Astrophys. J.* 479:L9–13

Annual Review of Astronomy and Astrophysics
Volume 43, 2005

CONTENTS